2021 1st Season Stock Assessment

Falkland calamari

(*Doryteuthis gahi*)

S1 - 2021 - LOL

Andreas Winter

Natural Resources - Fisheries
Falkland Islands Government
Stanley, Falkland Islands

June 2021

Index

Summary

1) The 2021 first season *Doryteuthis gahi* fishery (C license) was open from February 26th and closed by emergency order on April 28th. Compensatory flex days for mechanical breakdown and bad weather were voided after April 28th.
2) 59,587 tonnes of *D. gahi* catch were reported in the 2021 C-license fishery, giving an average CPUE of 66.9 t vessel-day^{-1}. Total catch was the highest for any season since 1995, and average CPUE was the highest since at least 2004. 58.1% of *D. gahi* catch and 57.6% of fishing effort were taken south of 52º S; 41.9% of *D. gahi* catch and 42.4% of fishing effort were taken north of 52º S.
3) In the south sub-area, four depletion periods / immigrations were inferred on February 26th (start of the season), March 29th, April 13th and April 23rd. In the north sub-area, fishing started on March 4th and two further depletion periods / immigrations were inferred on March 13th and March 30th.
4) Approximately 113,712 tonnes of *D. gahi* (95% confidence interval: 103,568 to 155,515 t) were estimated to have immigrated into the Loligo Box after the start of first season 2021, of which 55,313 t south of 52º S and 58,398 t north of 52º S.
5) The escapement biomass estimate for *D. gahi* remaining in the Loligo Box at the end of first season 2021 was: Maximum likelihood of 58,964 tonnes, with a 95% confidence interval of 50,346 to 96,683 tonnes.

   The risk of *D. gahi* escapement biomass at the end of the season being less than 10,000 tonnes was estimated at effectively zero.

Introduction

The first season (C licence) of the 2021 *Doryteuthis gahi* fishery (Patagonian longfin squid – colloquially *Loligo*) opened on February 26th, following a consensus two-day postponement for bad weather (Figure 1). Two vessels delayed entry to meet quarantining requirements and were temporarily replaced by alternate vessels. Throughout the season, 8 flex days were requested for mechanical breakdown, 2 for injury, and 12 for bad weather; all except one of the weather days were on March 11th (Figure 1).

All C-license vessels were required to embark an observer tasked to monitor presence and incidental capture of pinnipeds (Iriarte et al. 2020). The occurrence of two pinniped mortalities (one Southern sea lion *Otaria flavescens*, grid XVAK, and one South American fur seal *Arctocephalus australis*, grid XVAL) resulted in mandatory use of Seal Exclusion Devices (SEDs) south of 52° S starting on March 5th at 0001. Two further pinniped mortalities (one Southern elephant seal *Mirounga leonina*, grid XNAP, and one Southern sea lion, grid XNAP) resulted in mandatory use of SEDs north of 52° S starting on March 19th at 0001. At least one vessel had installed its SED from the start of the season (Evans 2021).

Similar to first season 2019 (Winter 2019a) and first season 2020 (Winter 2020), fishing was stopped early north of 52°S (on April 14th; decision on April 13th) because of small sizes of the *D. gahi* squid (Figure 2). North size distributions were scheduled for review after 14 days. Fishing was then stopped early south of 52°S (on April 28th; decision on April 27th) also because of small squid sizes (Figure 3), effectively triggering emergency closure of the fishing season. All outstanding flex days were voided by the closure.

Total reported *D. gahi* catch under first season C licence was 34,618 south + 24,969 north = 59,587 tonnes (Table 1), corresponding to an average CPUE of 59587 / 891 = 66.9 tonnes vessel-day^{-1}. Total catch was the highest for any season since 1995, and average CPUE was the highest since at least 2004.

Figure 1 [below]. Fish Ops chart display (right) and wind speed vector plots (Copernicus Marine Service) (left) on February 25th, one day before the postponed season opening, and on March 11th, when only three vessels fished.

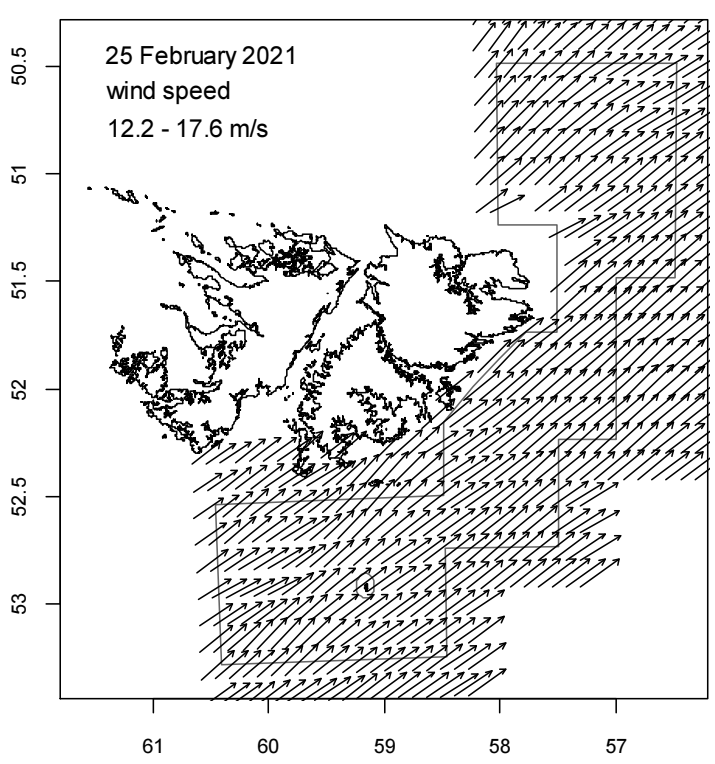

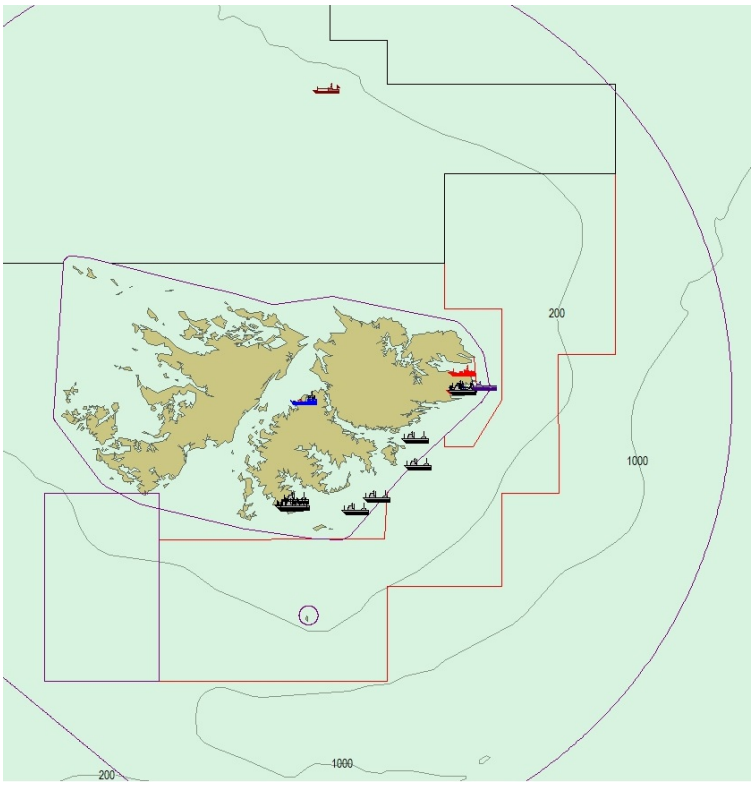

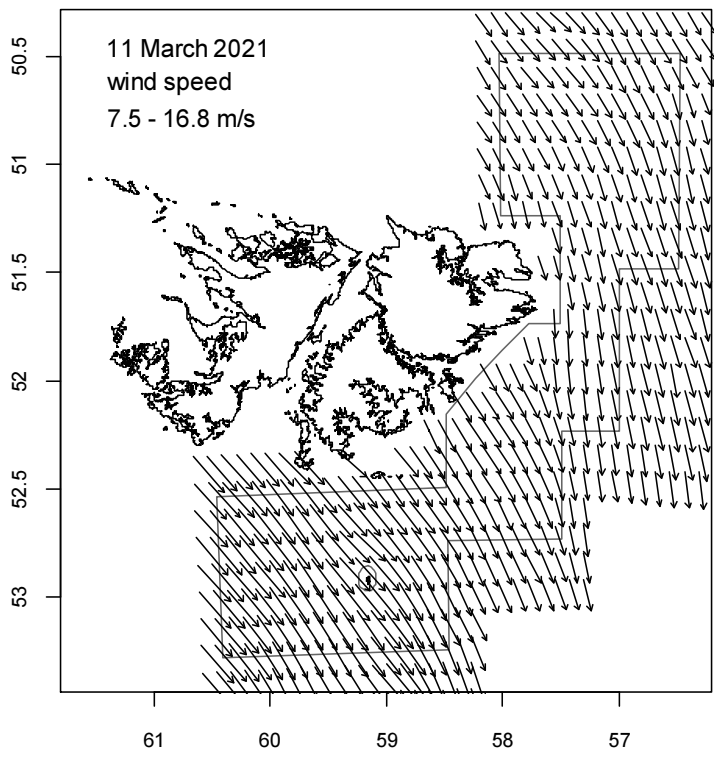

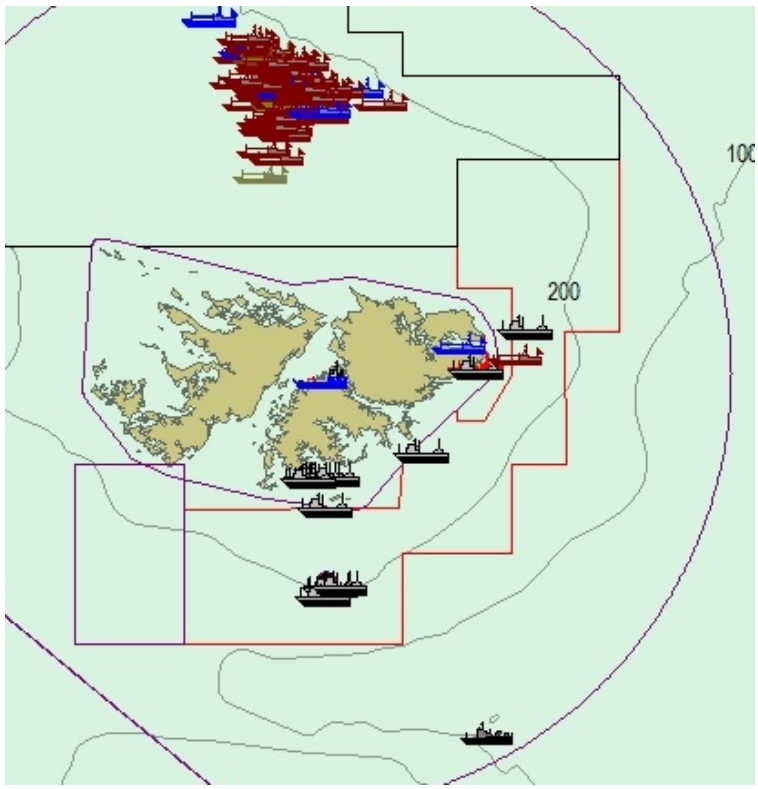

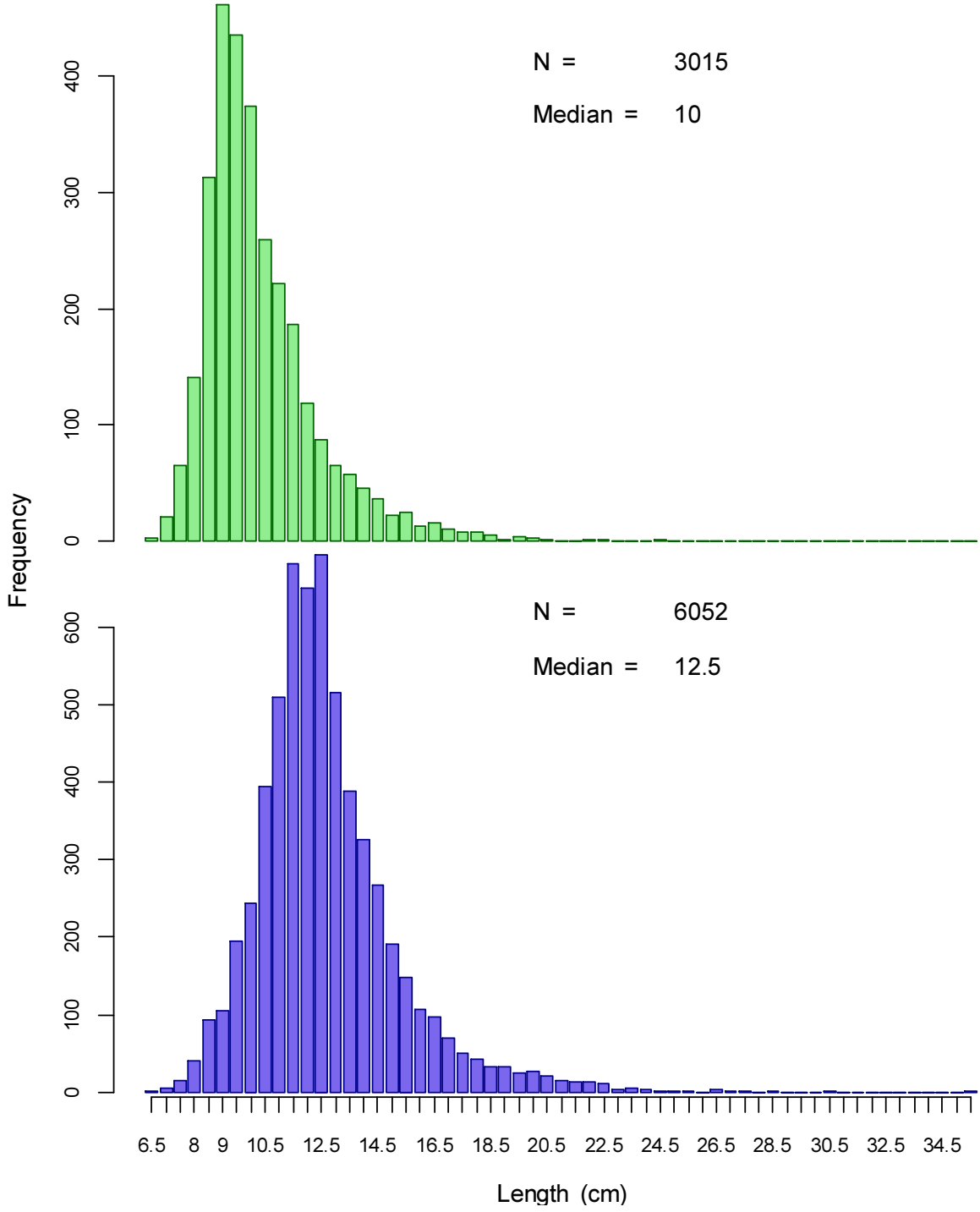

Figure 2. *D. gahi* observer length-frequency distributions from April 8th to April 12th 2021, the date range over which the decision was made to close the north sub-area on April 14th. In the north (green – top) 47.8% of individuals had mantle lengths < 10 cm. In the south (purple – bottom) 7.6% of individuals had mantle lengths < 10 cm.

Figure 3 [next page]. *D. gahi* observer length-frequency distributions from April 23rd to April 26th 2021, the date range over which the decision was made to close the south sub-area on April 28th. 34.9% of individuals had mantle lengths < 10 cm.

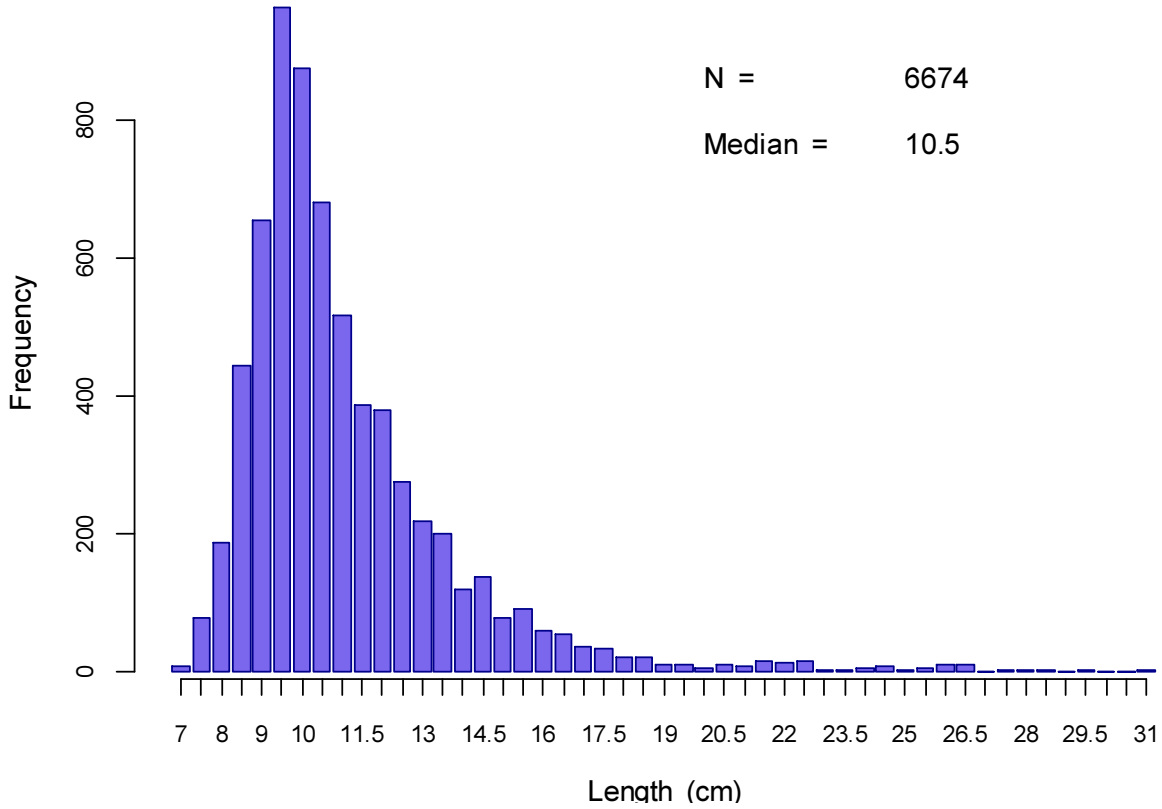

Table 1. *D. gahi* season comparisons since 2004, when catch management was assumed by the FIFD. Days: total number of calendar days open to licensed *D. gahi* fishing including (since 1st season 2013) optional extension days; V-Days: aggregate number of licensed *D. gahi* fishing days reported by all vessels for the season. Entries in italics are seasons closed by emergency order.

	Season 1			Season 2		
	Catch (t)	Days	V-Days	Catch (t)	Days	V-Days
2004	7,152	46	625	17,559	78	1271
2005	24,605	45	576	29,659	78	1210
2006	19,056	50	704	*23,238*	*53*	*883*
2007	17,229	50	680	*24,171*	*63*	*1063*
2008	24,752	51	780	26,996	78	1189
2009	12,764	50	773	*17,836*	*59*	*923*
2010	28,754	50	765	36,993	78	1169
2011	15,271	50	771	*18,725*	*70*	*1099*
2012	34,767	51	770	35,026	78	1095
2013	19,908	53	782	19,614	78	1195
2014	28,119	59	872	19,630	71	1099
2015	*19,383**	*57**	*871**	*10,190*	*42*	*665*
2016	22,616	68	1020	23,089	68	1004
2017	39,433	68	999†	24,101	69	1002‡
2018	43,085	69	975	35,828	68	977
2019	55,586	68	953	*24,748*	*43*	*635*
2020	29,116	68	1012	29,759	69	993
2021	*59,587*	*62*	*891*			

* Does not include C-license catch or effort after the target was switched from *D. gahi* to *Illex*.
† Includes two vessel-days of experimental fishing for juvenile toothfish.
‡ Includes one vessel-day of experimental fishing for juvenile toothfish.

Assessment of the Falkland Islands *D. gahi* stock was conducted with depletion time-series models as in previous seasons (Agnew et al. 1998, Roa-Ureta and Arkhipkin 2007; Arkhipkin et al. 2008), and in other squid fisheries (cited in Arkhipkin et al. 2020). Because *D. gahi* has an annual life cycle (Patterson 1988, Arkhipkin 1993), stock cannot be derived from a standing biomass carried over from prior years (Rosenberg et al. 1990, Pierce and Guerra 1994). The depletion model instead calculates an estimate of population abundance over time by evaluating what levels of abundance and catchability must be present to sustain the observed rate of catch. Depletion modelling of the *D. gahi* target fishery is used both in-season and for the post-season summary, with the objective of maintaining an escapement biomass of 10,000 tonnes *D. gahi* at the end of each season as a conservation threshold (Agnew et al. 2002, Barton 2002).

Methods

The depletion model formulated for the Falklands *D. gahi* stock is based on the equivalence:

$$C_{day} = q \times E_{day} \times N_{day} \times e^{-M/2} \quad \textbf{(1)}$$

where q is the catchability coefficient, M is the natural mortality rate (considered constant at 0.0133 day^{-1}; Roa-Ureta and Arkhipkin 2007), and C_{day}, E_{day}, N_{day} are respectively catch (numbers of squid), fishing effort (numbers of vessels), and abundance (numbers of squid) per day. The catchability coefficient q summarized the range of variation of all trawls taken by the fishing fleet in this season. Previous analysis had shown that no significant improvement in biomass estimation is produced by differentiating between trawls taken with SED and trawls taken without SED (Winter 2019a).

In its basic form (DeLury 1947) the depletion model assumes a closed population in a fixed area for the duration of the assessment. However, the assumption of a closed population is imperfectly met in the Falkland Islands fishery, where stock analyses have often shown that *D. gahi* groups arrive in successive waves after the start of the season (Roa-Ureta 2012; Winter and Arkhipkin 2015). Arrivals of successive groups are inferred from discontinuities in the catch data. Fishing on a single, closed cohort would be expected to yield gradually decreasing CPUE, but gradually increasing average individual sizes, as the squid grow. When instead these data change suddenly, or in contrast to expectation, the immigration of a new group to the population is indicated (Winter and Arkhipkin 2015).

In the event of a new group arrival, the depletion calculation must be modified to account for this influx. This is done using a simultaneous algorithm that adds new arrivals on top of the stock previously present, and posits a common catchability coefficient for the entire depletion time-series. If two depletions are included in the same model (i.e., the stock present from the start plus a new group arrival), then:

$$C_{day} = q \times E_{day} \times (N1_{day} + (N2_{day} \times i2|_0^1)) \times e^{-M/2} \quad \textbf{(2)}$$

where i2 is a dummy variable taking the values 0 or 1 if 'day' is before or after the start day of the second depletion. For more than two depletions, $N3_{day}$, i3, $N4_{day}$, i4, etc., would be included following the same pattern.

The season depletion likelihood function was calculated as the difference between actual catch numbers reported and catch numbers predicted from the model (Equation **2**),

statistically corrected by a factor relating to the number of days of the depletion period (Roa-Ureta 2012):

$$\text{minimization} \rightarrow \left((n\text{Days} - 2)/2\right) \times \log\left(\sum_{days}\left(\log(\text{predicted } C_{day}) - \log(\text{actual } C_{day})\right)^2\right) \quad \textbf{(3)}$$

The stock assessment was set in a Bayesian framework (Punt and Hilborn 1997), whereby results of the season depletion model are conditioned by prior information on the stock; in this case the information from the pre-season survey.

The likelihood function of prior information was calculated as the normal distribution of the difference between catchability derived from the survey abundance estimate ($_{prior}$ q), and catchability derived from the season depletion model ($_{depletion}$ q). Applying this difference requires both the survey and the season to be fishing the same stock with the same gear. Catchability, rather than abundance N, is used for calculating prior likelihood because catchability informs the entire season time series; whereas N from the survey only informs the first in-season depletion period – subsequent immigrations and depletions are independent of the abundance that was present during the survey. Thus, the prior likelihood function was:

$$\text{minimization} \rightarrow \frac{1}{\sqrt{2\pi \cdot SD_{prior\ q}{}^2}} \times \exp\left(-\frac{\left(_{depletion}\,q - {}_{prior}\,q\right)^2}{2 \cdot SD_{prior\ q}{}^2}\right) \quad \textbf{(4)}$$

where the standard deviation of catchability prior ($SD_{prior\ q}$) was calculated from the Euclidean sum (Carlson 2014) of the survey prior estimate uncertainty, the variability in catches on the season start date, and the uncertainty in the natural mortality M estimate over the number of days mortality discounting (Appendix Equations **A5**).

Bayesian optimization of the depletion was calculated by jointly minimizing Equations **3** and **4**, using the Nelder-Mead algorithm in R programming package 'optimx' (Nash and Varadhan 2011). Equations 3 and 4 were weighted equally, as the combination of high abundance and shortened season produced relatively "shallow" depletions which needed strong influence of the prior to optimize on realistic values. Because a complex model with multiple depletions may converge on a local minimum rather than global minimum, the optimization was stabilized by running a feed-back loop that set the q and N parameter outputs of the Bayesian joint optimization back into the in-season-only minimization (Equation **3**), re-calculated the in-season-only minimization, then re-calculated the Bayesian joint optimization, and continued this process until both the in-season minimization and the joint optimization remained unchanged.

With actual C_{day}, E_{day} and M being fixed parameters, the optimization of Equation **2** using Equations **3** and **4** produces estimates of q and N1, N2, …, etc. Numbers of squid on the final day (or any other day) of a time series are then calculated as the numbers N of the depletion start days discounted for natural mortality during the intervening period, and subtracting cumulative catch also discounted for natural mortality (CNMD). Taking for example a two-depletion period:

$$\begin{aligned} N_{final\ day} &= N1_{start\ day\ 1} \times e^{-M\ (final\ day - start\ day\ 1)} \\ &+ N2_{start\ day\ 2} \times e^{-M\ (final\ day - start\ day\ 2)} \\ &- CNMD_{final\ day}, \end{aligned} \quad \textbf{(5)}$$

$$CNMD_{day\ 1} = 0$$

$$CNMD_{day\ x} = CNMD_{day\ x-1} \times e^{-M} + C_{day\ x-1} \times e^{-M/2} \quad \textbf{(6)}$$

$N_{\text{final day}}$ is then multiplied by the average individual weight of squid on the final day to give biomass. Daily average individual weight is obtained from length / weight conversion of mantle lengths measured in-season by observers, and also derived from in-season commercial data as the proportion of product weight that vessels reported per market size category[a]. Observer mantle lengths are scientifically more accurate, but restricted to a partial sample of trawls. Commercially proportioned mantle lengths are relatively less accurate, but cover every trawl of the entire fishing fleet every day. Therefore, both sources of data are used (see Appendix – *Doryteuthis gahi* individual weights).

Distributions of the likelihood estimates from joint optimization (i.e., measures of their statistical uncertainty) were computed using a Markov Chain Monte Carlo (MCMC) (Gamerman and Lopes 2006), a method that is commonly employed for fisheries assessments (Magnusson et al. 2013). MCMC is an iterative process which generates random stepwise changes to the proposed outcome of a model (in this case, the q and N of *D. gahi* squid) and at each step, accepts or nullifies the change with a probability equivalent to how well the change fits the model parameters compared to the previous step. The resulting sequence of accepted or nullified changes (i.e., the 'chain') approximates the likelihood distribution of the model outcome. The MCMC of the depletion models were run for 200,000 iterations; the first 1000 iterations were discarded as burn-in sections (initial phases over which the algorithm stabilizes); and the chains were thinned by a factor equivalent to the maximum of either 5 or the inverse of the acceptance rate (e.g., if the acceptance rate was 12.5%, then every 8^{th} (0.125^{-1}) iteration was retained) to reduce serial correlation. For each model three chains were run; one chain initiated with the parameter values obtained from the joint optimization of Equations **3** and **4**, one chain initiated with these parameters ×2, and one chain initiated with these parameters ×¼. Convergence of the three chains was accepted if the variance among chains was less than 10% higher than the variance within chains (Brooks and Gelman 1998). When convergence was satisfied the three chains were combined as one final set. Equations **5**, **6**, and the multiplication by average individual weight were applied to the CNMD and to each iteration of N values in the final set, and the biomass outcomes from these calculations represent the distribution of the estimate.

Depletion models and likelihood distributions were calculated separately for north and south sub-areas of the Loligo Box fishing zone, as *D. gahi* sub-stocks emigrate from different spawning grounds and remain to an extent segregated (Arkhipkin and Middleton 2002). However, the algorithm was changed this season in calculating q_{prior} for the north and south sub-areas combined, rather than separately (Equation **A4**). As fishing tends to start predominantly in one or the other sub-area, rather than the fleet spreading itself evenly, separately computed north and south qs_{prior} were susceptible to arbitrary differences. Total escapement biomass was then defined as the aggregate biomass of *D. gahi* on the last day of the season for north and south sub-areas combined. North and south biomasses are not assumed to be uncorrelated however (Shaw et al. 2004), and therefore north and south likelihood distributions were added semi-randomly in proportion to the strength of their day-to-day correlation (see Winter 2014, for the semi-randomization algorithm).

Figure 4 [next page]. Spatial distribution of *D. gahi* 1^{st}-season trawls, colour-scaled to catch weight (max. = 94.1 tonnes). 2341 trawl catches were taken during the season. The 'Loligo Box' fishing zone and 52 ºS parallel delineating the boundary between north and south assessment sub-areas, are shown in grey.

[a] First reported for Falkland Islands *D. gahi* by Payá (2006). Also used in some finfish commercial fisheries, see Plet-Hansen et al. 2018.

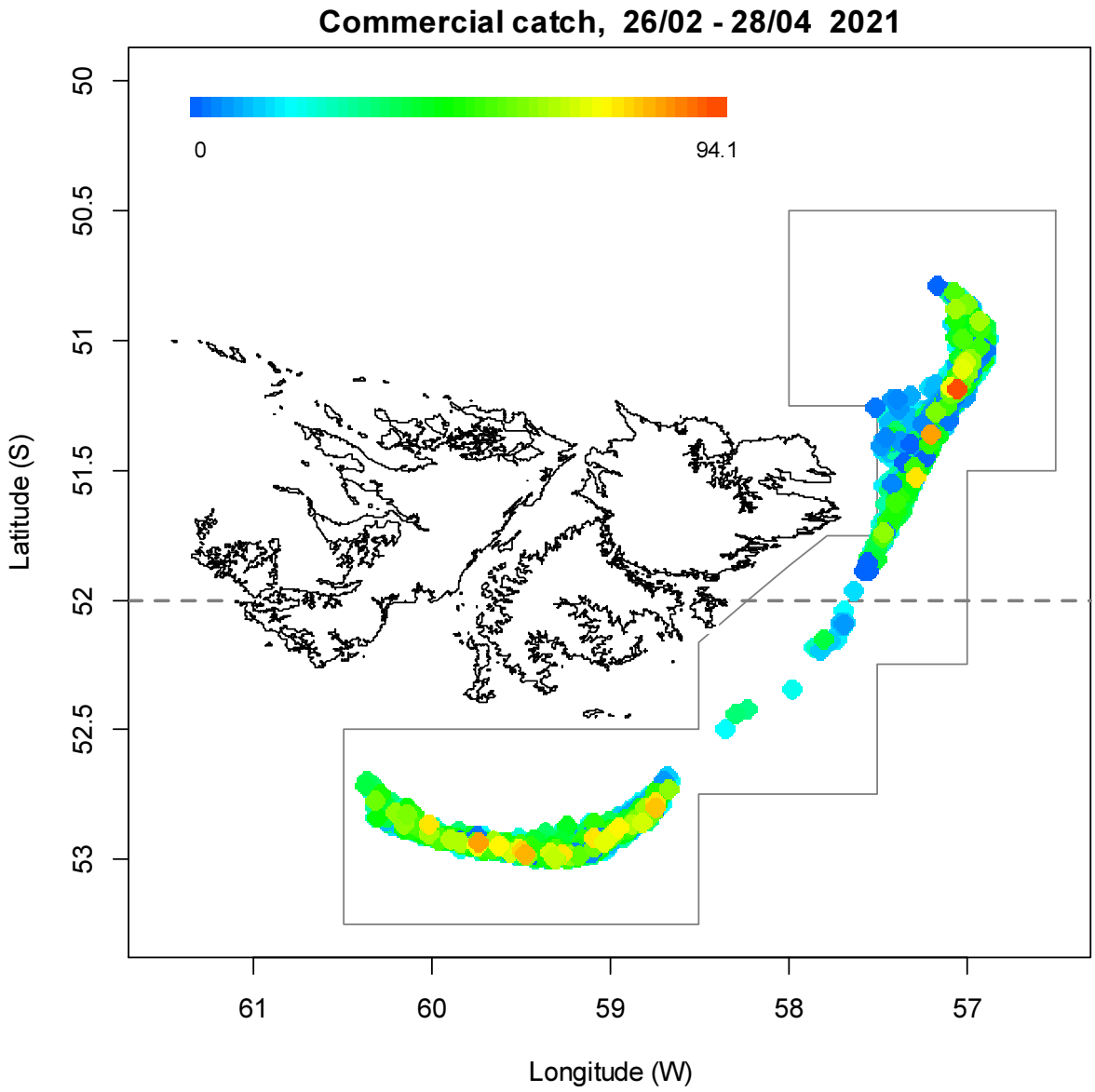

Stock assessment

Catch and effort

The north sub-area was fished on 40 of 62 season-days, for 41.9% of total catch (24969.3 t *D. gahi*) and 42.4% of effort (377.7 vessel-days) (Figures 4 and 5). Two trawls in the north, both on March 15th, reported broken nets on haul and the observer's or fishing master's visual estimates of *D. gahi* catch lost at sea were added to the production report totals. The south sub-area was fished on 47 of the 62 season-days, for 58.1% of total catch (34618.0 t *D. gahi*) and 57.6% of effort (513.3 vessel-days). The season was characterized by strong alternation between the fleet fishing north and south: over the first 15 days 98.1% of *D. gahi* catch vs. 95.8% of effort was taken south, over 25 days through the middle 89.9% of *D. gahi* catch vs. 90.0% of effort was taken north, and the final 15 days were 100% south by order. Out of 47 season days that were open both north and south, 34 days had >90% of *D. gahi* catch and 33 days had >90% of effort on just one side of 52°S or the other. Correspondingly the *D. gahi* catch distribution was strongly decentred (Figure 4) compared to both seasons last year (Winter 202a, 202b), with only 0.5% of total catch taken between 52°S and 52.5°S; the

historically defined central sub-area of the Loligo Box (e.g., Figure 2 in Roa-Ureta and Arkhipkin 2007).

With the *Illex* fishing season concurrently underway, substantial catches of *Illex argentinus* were reported by vessels on several days (Figure 5), raising concerns of a reprise of the *Illex* Loligo Box ingressions in 2011 (Winter 2011) and especially 2015 (Winter 2015). However, *Illex* ultimately did not amount to a serious issue in this season as a total of just 294.9 tonnes were reported caught in the north sub-area and 11.1 t in the south sub-area.

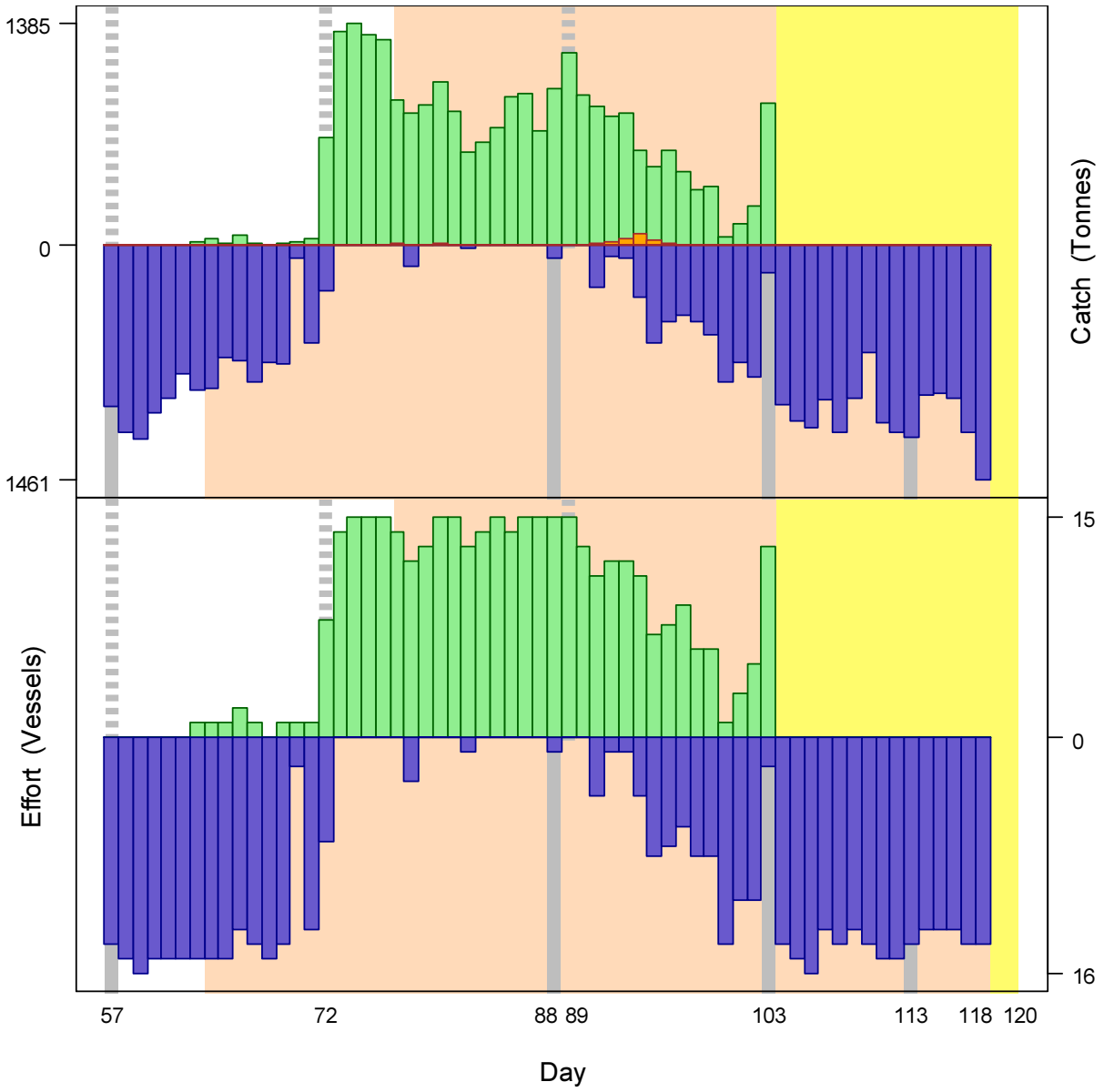

Figure 5. Daily total *D. gahi* catch and effort distribution by assessment sub-area north (green) and south (purple) of the 52° S parallel during 1st season 2021. Orange bars: *I. argentinus* catch. The season was open from February 26th (chronological day 57) with directed closure scheduled on April 30th (day 120), but closed by emergency order after April 28th (day 118). Tan under-shading: mandatory use of SEDs north and south. Yellow under-shading: early closures of the north and south sub-areas. As many as 15 vessels fished per day north; as many as 16 vessels fished per day south. As much as 1,385 tonnes *D. gahi* was caught per day north; as much as 1,461 tonnes *D. gahi* was caught

per day south. As much as 75 tonnes *I. argentinus* was caught per day north; as much as 2 tonnes *I. argentinus* was caught per day south.

Data

891 vessel-days were fished during the season (Table 1), with a median of 15 vessels per day (mean 14.4). Vessels reported daily catch totals to the FIFD and electronic logbook data that included trawl times, positions, depths, and product weight by market size categories. Four FIG fishery observers were deployed on three vessels in the fishing season for a total of 51 sampling days[b] (Evans 2021, Brewin 2021, Claes 2021, Tutjavi 2021). Throughout the 62 days of the season, 16 days had no FIG fishery observer covering, 41 days had 1 FIG fishery observer covering, and 5 days had two FIG fishery observers covering. Except for seabird days FIG fishery observers were tasked with sampling 200 *D. gahi* at two stations daily; reporting their maturity stages, sex, and lengths to 0.5 cm. Contract marine mammal observers were tasked with measuring 200 unsexed lengths of *D. gahi* per day. The length-weight relationship for converting observer and commercially proportioned lengths was combined from 1st pre-season and season length-weight data of both 2020 and 2021, as 2021 data became available progressively with on-going observer coverage. The final parameterization of the length-weight relationship included 2973 measures from 2020 and 4390 measures from 2021, giving:

$$\text{weight (kg)} = 0.22410 \times \text{length (cm)}^{2.11095} / 1000 \quad \textbf{(7)}$$

with a coefficient of determination $R^2 = 94.3\%$.

Group arrivals / depletion criteria

Start days of depletions - following arrivals of new *D. gahi* groups - were judged primarily by daily changes in CPUE, with additional information from sex proportions, maturity, and average individual squid sizes. CPUE was calculated as metric tonnes of *D. gahi* caught per vessel per day. Days were used rather than trawl hours as the basic unit of effort. Commercial vessels do not trawl standardized duration hours, but rather durations that best suit their daily processing requirements. An effort index of days is therefore more consistent (FIFD 2004, Winter and Arkhipkin 2015). For the first time this season, inclusion of additional depletion starts was evaluated by improvement of the Akaike information criterion (Akaike 1973) on model fit, relative to the fewer depletion starts.

Four days in the south and three days in the north were identified that represented the onset of separate immigrations / depletions throughout the season.

- The first depletion start south was set on day 57 (February 26th), the first day of the season with fourteen vessels fishing south. CPUE was near its maximum for the first half of the season (Figure 6). Average individual observer weights (Figure 7B) and average maturities (Figure 7D) were near their minima for the season.
- The second depletion start south was identified on day 88 (March 29th). A single vessel fished south that day, making the explicit date of immigration uncertain. That

[b] Not counting seabird days (every fourth day).

single vessel had the highest average commercial weight all season (Figure 7A), and the highest CPUE since 30 days earlier (Figure 6).

- The third depletion start south was identified on day 103 (April 13th). CPUE (from two vessels) was the highest all season up to that date (Figure 6), and average individual weights showed pronounced dips (Figures 7A, 7B).
- The fourth depletion start south was identified on day 113 (April 23rd). CPUE was highest since the third depletion start (Figure 6). Average individual weights again showed pronounced dips (Figures 7A, 7B) as did average maturities (Figure 7D), while the proportion of females suggested a peak (Figure 7C).
- The first depletion start north was assigned on day 57, the first day of the season, whereby fishing in the north did not start until day 63 (March 4th).
- The second depletion start north was identified on day 72 (March 13th) with a strong increase in CPUE (Figure 6). The proportion of females increased substantially after day 72 (Figure 7C).
- The third depletion start north was identified on day 89 (March 30th) following a sudden decrease in the proportion of females (Figure 7C) and with a strong increase to the highest CPUE since 13 days (Figure 6).

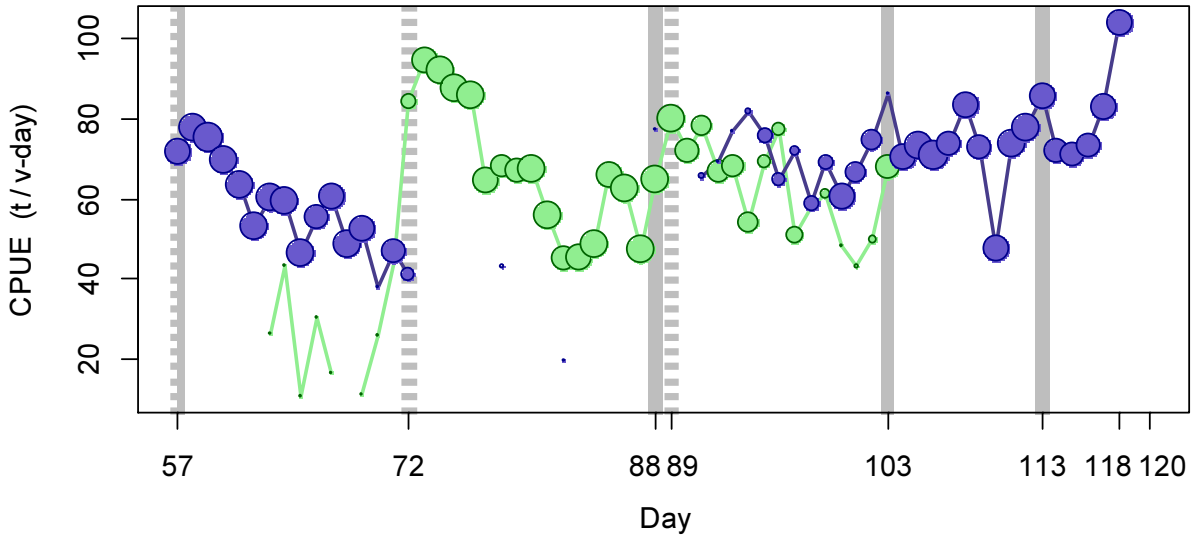

Figure 6. CPUE in metric tonnes per vessel per day, by assessment sub-area north (green) and south (purple) of 52° S latitude. Circle sizes are proportioned to numbers of vessels fishing. Data from consecutive days are joined by line segments. Broken grey bars indicate the starts of in-season depletions north. Solid grey bars indicate the starts of in-season depletions south.

Figure 7 [next page]. A: Average individual *D. gahi* weights (kg) per day from commercial size categories. B: Average individual *D. gahi* weights (kg) by sex per day from FIG observer sampling. C: Proportions of female *D. gahi* per day from observer sampling. D: Average maturity index value (Lipiński 1979) by sex per day from observer sampling. Males: triangles, females: squares, combined: circles. Thick lines (B) are unsexed measurements from the contract marine mammal observers. North sub-area: green, south sub-area: purple. Data from consecutive days are joined by line segments. Broken grey bars: the starts of in-season depletions north. Solid grey bars: the starts of in-season depletions south.

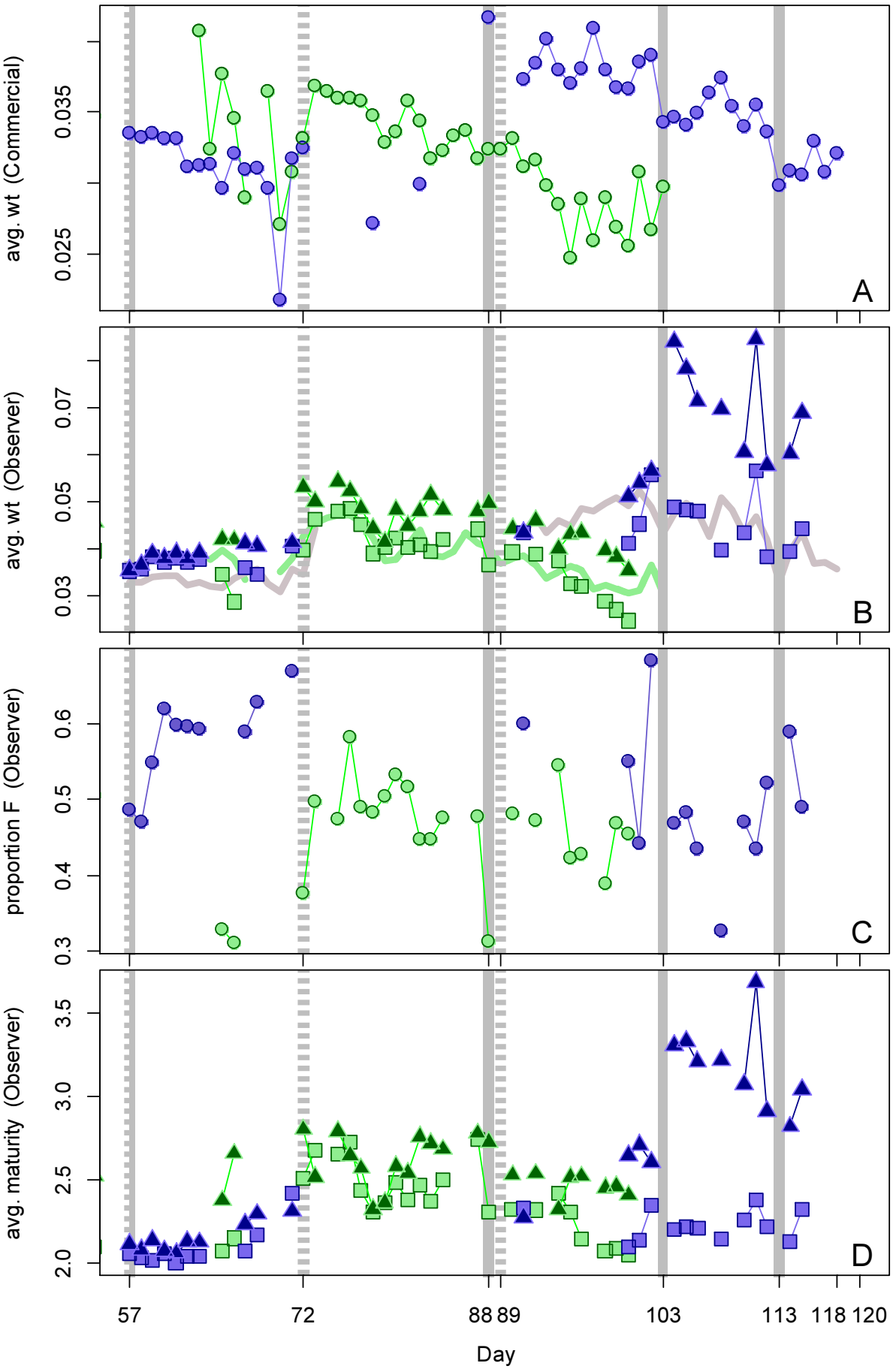
avg. wt (Commercial)
0.025
0.035
A
avg. wt (Observer)
0.03
0.05
0.07
B
proportion F (Observer)
0.3
0.4
0.5
0.6
C
avg. maturity (Observer)
2.0
2.5
3.0
3.5
D
57
72
88 89
103
113
118 120
Day

Average CPUE both surged to peaks on the last day of fishing open in either sub-area; in the case of the south sub-area the highest CPUE all season (Figure 6). These were however considered tactical catches, and not identified as further immigration events.

Depletion analyses
South

In the south sub-area, the maximum likelihood posterior ($_{\text{Bayesian}}\ q_S = 2.063 \times 10^{-3}$; Figure 8-left, and Equation **A7-S**) was almost exactly intermediate between the pre-season prior ($_{\text{prior}}\ q = 2.591 \times 10^{-3}$; Figure 8-left, and Equation **A4**) and the in-season depletion ($_{\text{depletion}}\ q_S = 1.556 \times 10^{-3}$; Figure 8-left, and **A6-S**).

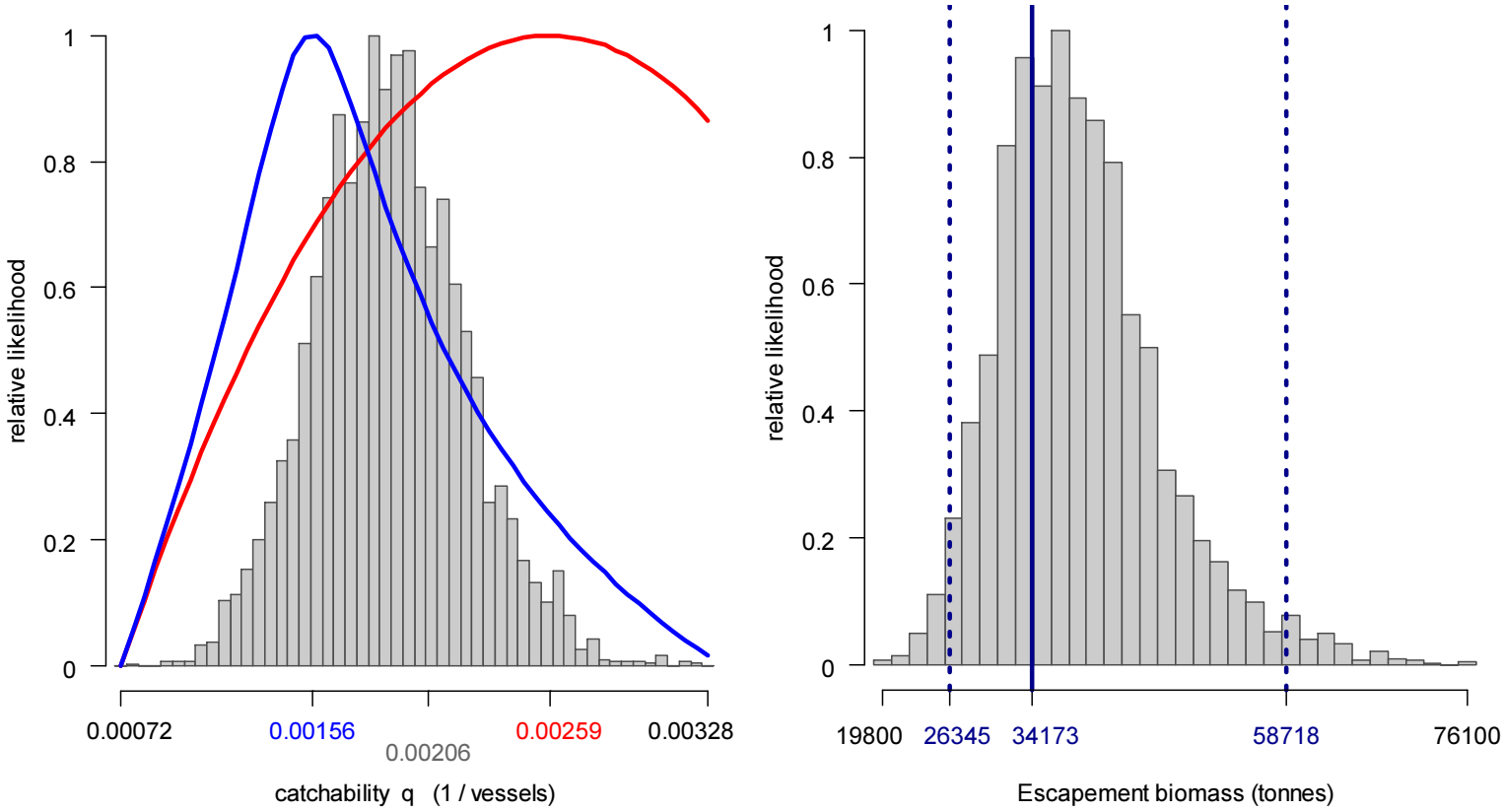

Figure 8. South sub-area. Left: Likelihood distributions for *D. gahi* catchability. Red line: prior model (pre-season survey data), blue line: in-season depletion model, grey bars: combined Bayesian model posterior. Right: Likelihood distribution (grey bars) of escapement biomass, from Bayesian posterior and average individual squid weight at the end of the season. Blue lines: maximum likelihood and 95% confidence interval. Note correspondence to Figure 9.

The MCMC distribution of the Bayesian posterior multiplied by the GAM fit of average individual squid weight (Figure A1-south) gave the likelihood distribution of *D. gahi* biomass on day 118 (April 28th) shown in Figure 8-right, with maximum likelihood and 95% confidence interval of:

$$B_{S\ \text{day}\ 118} = 34{,}173\ \text{t} \sim 95\%\ \text{CI}\ [26{,}345 - 58{,}718]\ \text{t} \qquad \textbf{(9-S)}$$

On the first day of the season estimated *D. gahi* biomass south was 39,314 t ~ 95% CI [33,180 – 58,105] t (Figure 9); higher than the pre-season estimate of 24,229 t [23,556 – 41,787] (Winter et al. 2021). As highest catches came relatively late during the survey, the scenario suggests that biomass was still accumulating during the early part of the season and was realistically higher than calculated from the survey. The highest biomass estimate of the season occurred with the fourth immigration on day 113, reaching 44,525 t [35,584 – 72,560]. However, the biomass time series trend variation was never statistically significant between the second immigration on day 88 and the end of the season, by the rule that a straight line could be drawn through the plot (Figure 9) without intersecting the 95% confidence interval (Swartzman et al. 1992).

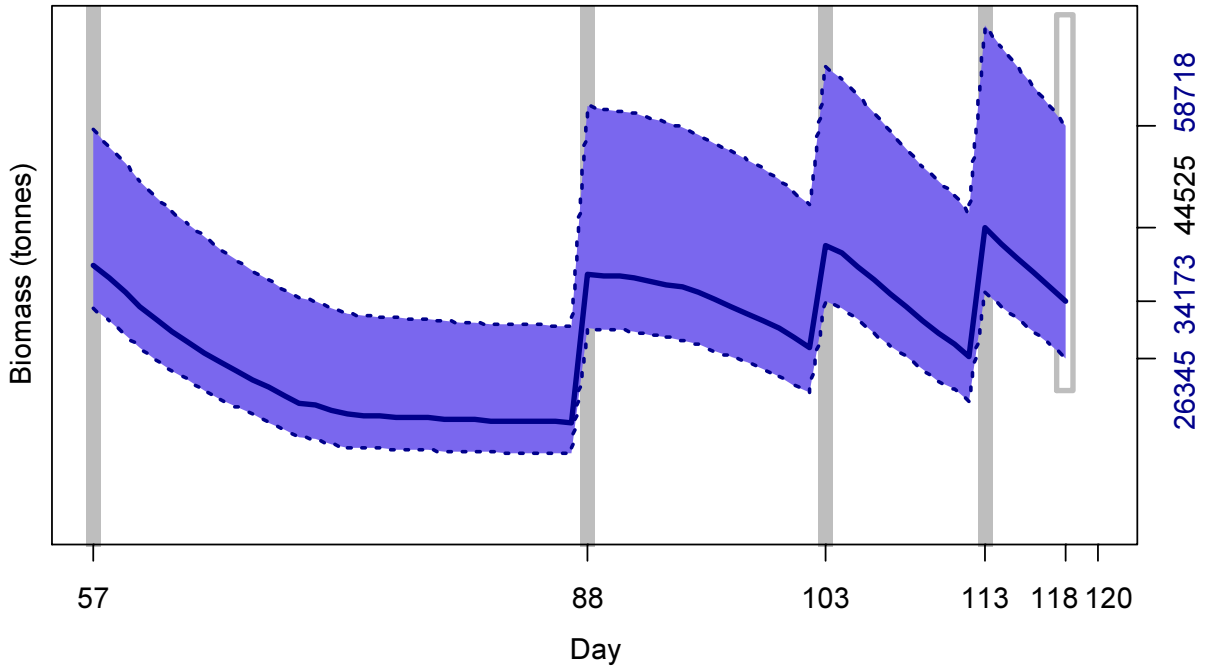

Figure 9. South sub-area. *D. gahi* biomass time series estimated from Bayesian posterior of the depletion model ± 95% confidence interval. Grey bars indicate the start of in-season depletions south; days 57, 88, 103 and 113. Note that the biomass 'footprint' on day 118 (April 28th) corresponds to the right-side plot of Figure 8.

North

In the north sub-area, the maximum likelihood posterior ($_{\text{Bayesian}}\, q_N = 2.030 \times 10^{-3}$; Figure 10-left, and Equation **A7-N**) was more closely modelled on the prior ($_{\text{prior}}\, q = 2.591 \times 10^{-3}$; Figure 10-left, and Equation **A4**) than on the in-season depletion ($_{\text{depletion}}\, q_N = 0.661 \times 10^{-3}$; Figure 10-left, and Equation **A6-N**).

Calculation of the *D. gahi* biomass distribution variation was augmented by an additional step. As fishing was stopped in the north 15 days earlier than the south, the absence of continuing measurements of individual sizes brought an increasingly high margin of error to the average size estimate over those last 15 days (Figure A1), translating to increased uncertainty of the corresponding catch numbers of individuals N per day. A relatively high margin of error was also evident over the first days of the season, as the later start of fishing in the north produced a gap of measurements at the start too (Figure A1). To

include this extra uncertainty, GAM-modelled average weights per day (Appendix – *Doryteuthis gahi* individual weights) were resampled as the empirical average weights plus their standard error multiplied by a randomly generated deviate drawn from the normal distribution with mean = 0 and standard deviation = 1[c]:

$$\text{R Avg}_{\text{Wt day}}\Big|_{\text{day}=57}^{\text{day}=118} = \text{Avg}_{\text{Wt day}}\Big|_{\text{day}=57}^{\text{day}=118} + \text{SE}_{\text{Wt day}}\Big|_{\text{day}=57}^{\text{day}=118} \times \sim\text{norm}(0, 1) \qquad \textbf{(8-N)}$$

One randomly generated deviate was applied to all days of the season time series, as average weights on successive days are not independent of each other[d]. Resampling was iterated 30,000×, and the variance of the resamples was added to the variance of the MCMC. Details are summarized in the Appendix – individual weight uncertainty. The added variance increased the width of the 95% confidence interval by about 1.0% at the start of the season and up to 9.6% at the end of the season, visible as the difference between pale green and light green on Figure 11.

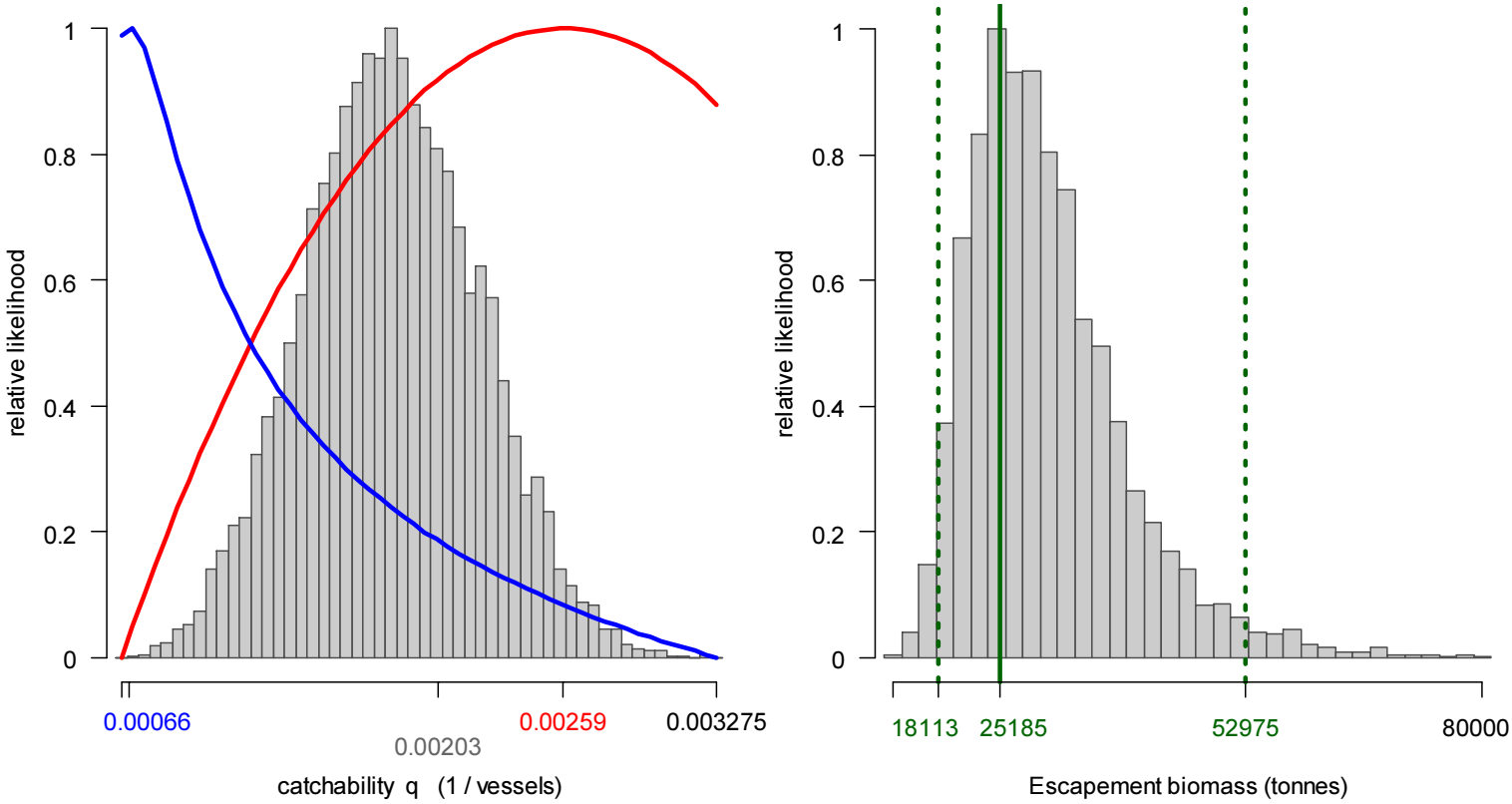

Figure 10. North sub-area. Left: Likelihood distributions for *D. gahi* catchability. Red line: prior model (pre-season survey data), blue line: in-season depletion model, grey bars: combined Bayesian model posterior. Right: Likelihood distribution (grey bars) of escapement biomass, from Bayesian posterior and average individual squid weight at the end of the season. Green lines: maximum likelihood and 95% confidence interval. Note the correspondence to Figure 11.

[c] With mean = 0, a randomly generated deviate is as likely negative as positive. For comparison, the commonly referenced 95% confidence interval is 1.96 standard deviations assuming a normal distribution (Rohlf and Sokal 1981).

[d] Before and after a new immigration they are arguably semi-independent, but the complexity of modelling semi-independence was judged unnecessary.

The MCMC distribution plus average individual weight variation gave the likelihood distribution of *D. gahi* biomass on day 118 (April 28th) shown in Figure 10-right, with maximum likelihood and 95% confidence interval of:

$$B_{N\ day\ 118} = 25{,}185\ t \sim 95\%\ CI\ [18{,}113 – 52{,}975]\ t \quad \textbf{(9-N)}$$

Note that the biomass trend is slightly increasing over the end of the season up to day 118 (Figure 11), as growth of the squid outweighs natural mortality in the absence of any more commercial fishing. On the first day of the season estimated *D. gahi* biomass north was 12,146 t ~ 95% CI [9,217 – 23,456] t (Figure 11). As in the south, this in-season biomass estimate was higher than the pre-season estimate of 7,541 t [4,655 – 12,779] (Winter et al. 2021). The depletion model fit quite well through the low-effort early part of the season (Figure A2-N), but one potential bias in the data is that vessels may fish just after leaving port, and thereby still be positioned in the north, opportunistically but without expectation of maximizing their catch. The highest biomass estimate of the season occurred with the second immigration on day 72, reaching 45,029 t [36,923 – 77,165], slightly more than with the third immigration on day 89: 43,166 t [34,741 – 76,271].

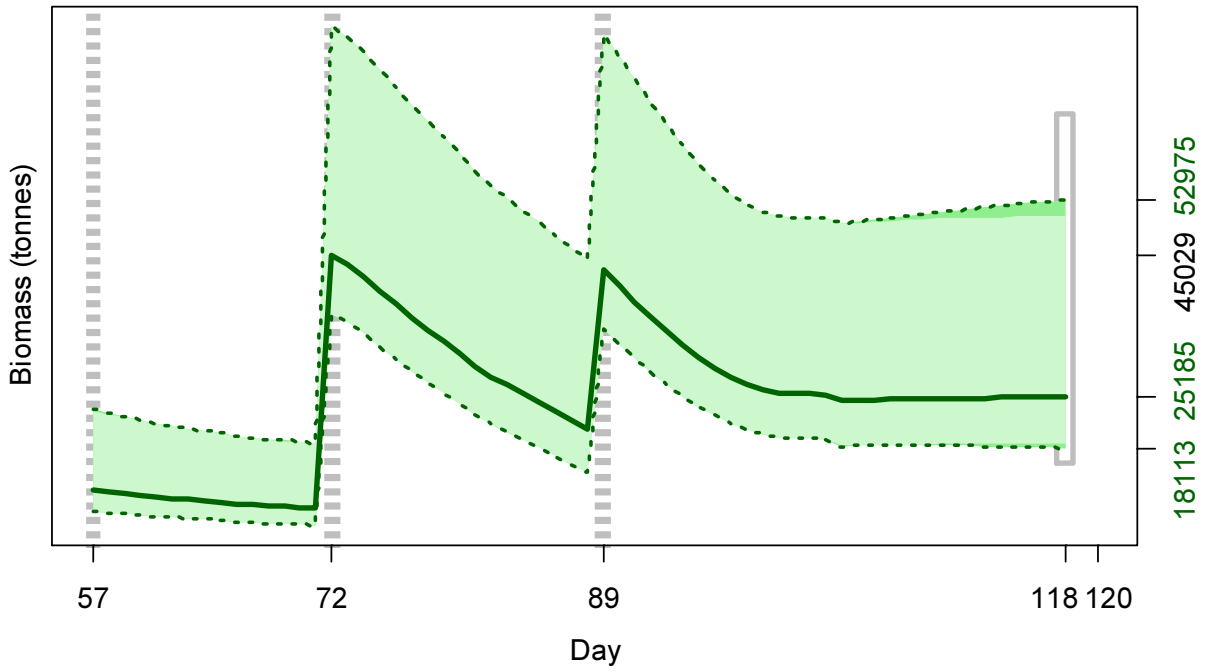

Figure 11. North sub-area. *D. gahi* biomass time series estimated from Bayesian posterior of the depletion model ± 95% confidence interval. Light green covers the confidence interval that includes variability of the average individual weight estimate; overlaid pale green covers the confidence interval without variability of the average individual weight estimate. Broken grey bars indicate the start of in-season depletions north; days 57, 72 and 89. Note that the biomass 'footprint' on day 118 (April 28th) corresponds to the right-side plot of Figure 10.

Immigration

Doryteuthis gahi immigration during the season was inferred on each day by how many more squid were estimated present than the day before, minus the number caught and the number expected to have died naturally:

$$_{\text{Immigration}}N_{\text{day i}} = N_{\text{day i}} - (N_{\text{day i-1}} - C_{\text{day i-1}} - M_{\text{day i-1}})$$

where $N_{\text{day i-1}}$ are optimized in the depletion models, $C_{\text{day i-1}}$ calculated as in Equation **3**, and $M_{\text{day i-1}}$ is:

$$M_{\text{day i-1}} = (N_{\text{day i-1}} - C_{\text{day i-1}}) \times (1 - e^{-M})$$

Immigration biomass per day was then calculated as the immigration number per day multiplied by predicted average individual weight from the GAM:

$$_{\text{Immigration}}B_{\text{day i}} = {}_{\text{Immigration}}N_{\text{day i}} \times {}_{\text{GAM}}Wt_{\text{day i}}$$

All numbers N are themselves derived from the daily average individual weights, therefore the estimation automatically factors in that those squid immigrating on a given day would likely be smaller than average (because younger). Confidence intervals of the immigration estimates were calculated by applying the above algorithms to the MCMC iterations of the depletion models, and for the north sub-area, including the individual weight uncertainty; cf. Equation **8-N**). Resulting total biomasses of *D. gahi* immigration north and south, up to season end (day 118), were:

$$_{\text{Immigration}}B_{\text{S season}} = 55{,}313 \text{ t} \sim 95\% \text{ CI } [\ 47{,}476 \text{ to } 79{,}027] \text{ t} \quad \textbf{(10-S)}$$

$$_{\text{Immigration}}B_{\text{N season}} = 58{,}398 \text{ t} \sim 95\% \text{ CI } [\ 49{,}353 \text{ to } 92{,}322] \text{ t} \quad \textbf{(10-N)}$$

Total immigration with semi-randomized addition of the confidence intervals was:

$$_{\text{Immigration}}B_{\text{Total season}} = 113{,}712 \text{ t} \sim 95\% \text{ CI } [103{,}568 \text{ to } 155{,}515] \text{ t} \quad \textbf{(10-T)}$$

In the south sub-area, the in-season peaks on days 88, 103, and 113 accounted for approximately 36.5%, 26.8%, and 34.2% of in-season immigration (start day 57 was de facto not an in-season immigration). The minor 'bumps' throughout the season, visible on Figure 9, accounted for the remaining 2.5%. In the north sub-area, the in-season peaks on days 72 and 89 accounted for approximately 59.1% and 39.2% of in-season immigrations.

Escapement biomass

Total escapement biomass was defined as the aggregate biomass of *D. gahi* at the end of day 118 (April 28th) for south and north sub-areas combined (Equations **9-S** and **9-N**). Depletion models are calculated on the inference that all fishing and natural mortality are gathered at mid-day, thus a half day of mortality ($e^{-M/2}$) was added to correspond to the closure of the fishery at 23:59 (mid-night) on April 28th for the final remaining vessel: Equation **11**.

$$B_{\text{Total day 118}} = (B_{\text{S day 118}} + B_{\text{N day 118}}) \times e^{-M/2}$$

$$= 59{,}358 \text{ t} \times 0.99336$$

$$= 58{,}964 \text{ t} \sim 95\% \text{ CI } [50{,}346 - 96{,}683] \text{ t} \quad \textbf{(11)}$$

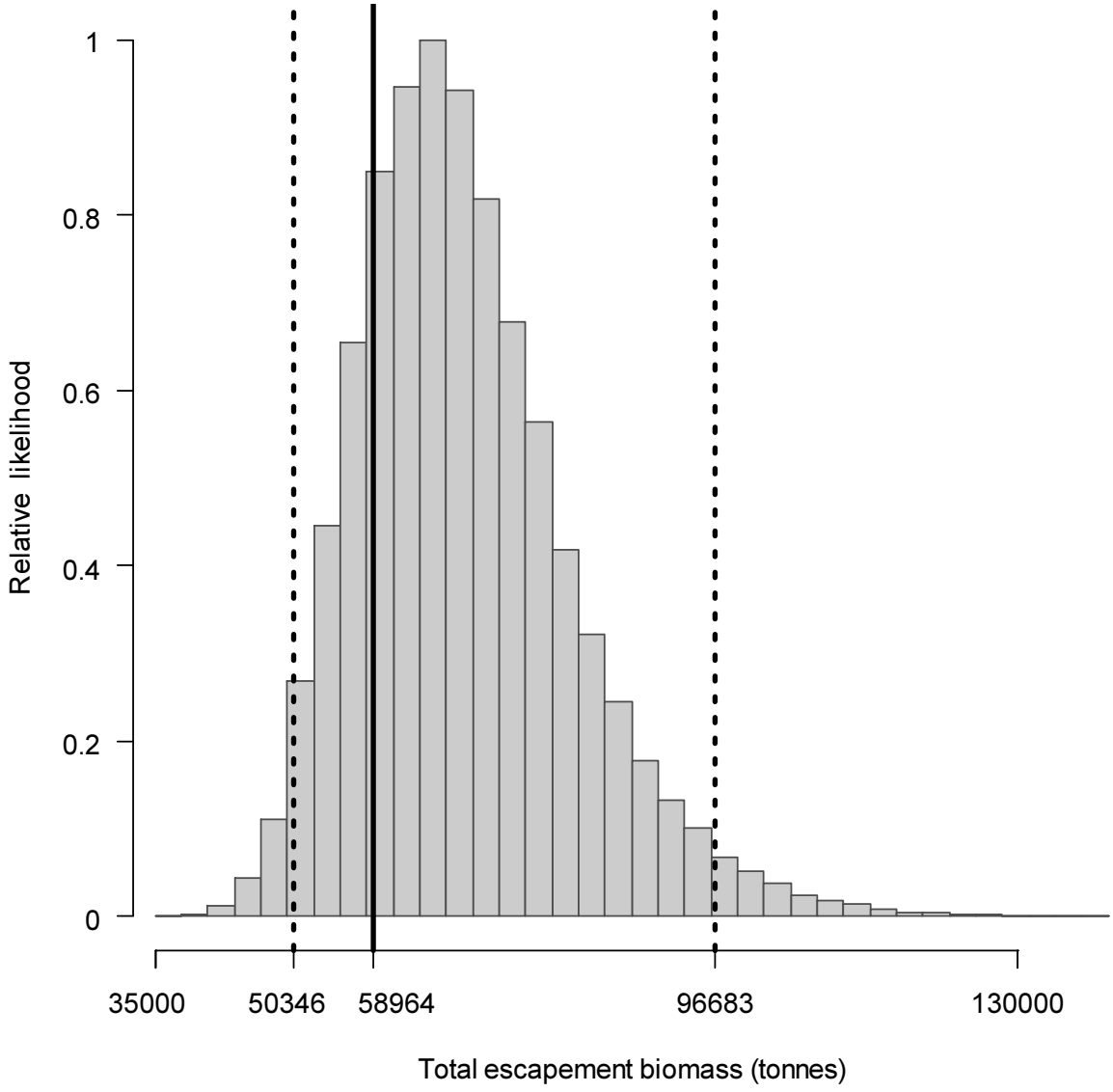

Figure 12. Likelihood distribution with 95% confidence interval of total *D. gahi* escapement biomass at the season end (April 28th).

South and north biomass season time series were not significantly correlated with each other, at R = –0.0703). Semi-randomized addition of the south and north distributions gave the aggregate likelihood of total escapement biomass ($B_{\text{Total day 118}}$) shown in Figure 12. With the absence of correlation between north and south biomass time series, and the weak depletion trends (Figures 9 and 11), the empirical estimate of $B_{\text{Total day 118}}$ was not centred on the median of the variability distribution. The estimated escapement biomass of 58,964 t was the highest for any season closed by emergency order since at least 2005. The risk of the fishery in the current season, defined as the proportion of the total escapement biomass distribution below the conservation limit of 10,000 tonnes (Agnew et al. 2002, Barton 2002), was effectively zero. For comparison, the minimum aggregate biomass of the season was estimated on day 71 (March 12th) as 29,472 t (95% confidence interval 24,912 to 46,693 t); also with zero risk of < 10,000 tonnes.

Fishery bycatch

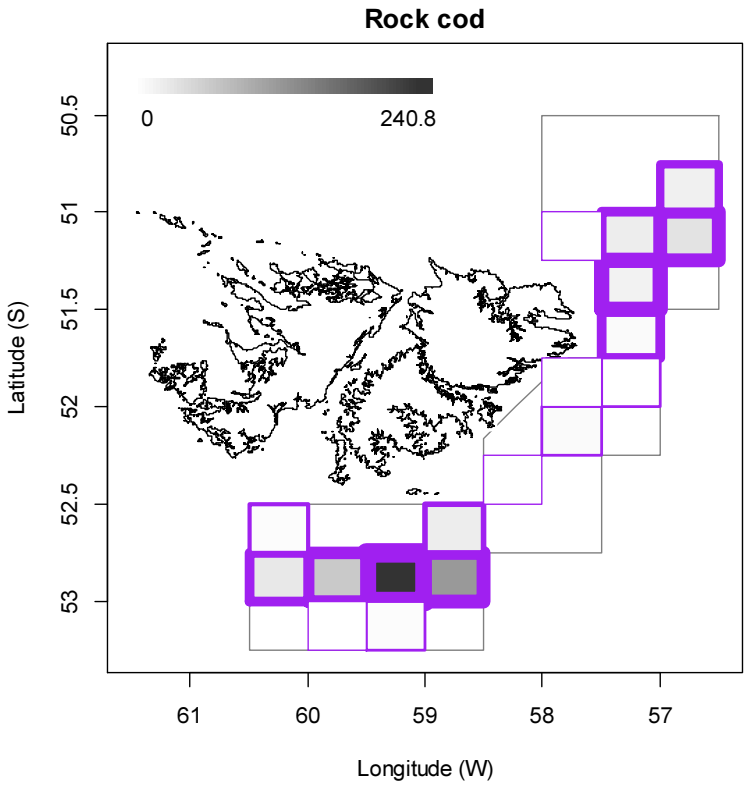

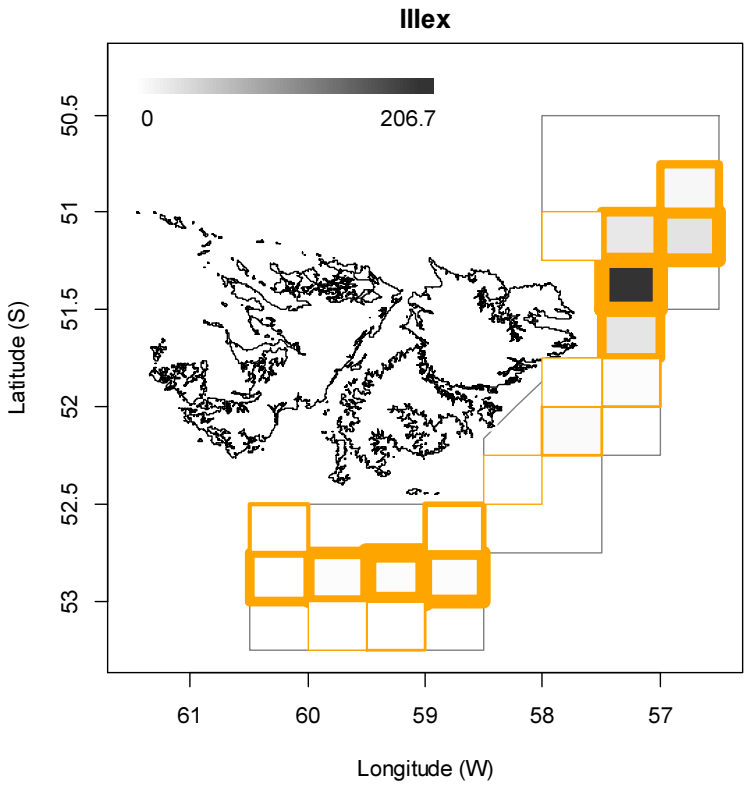

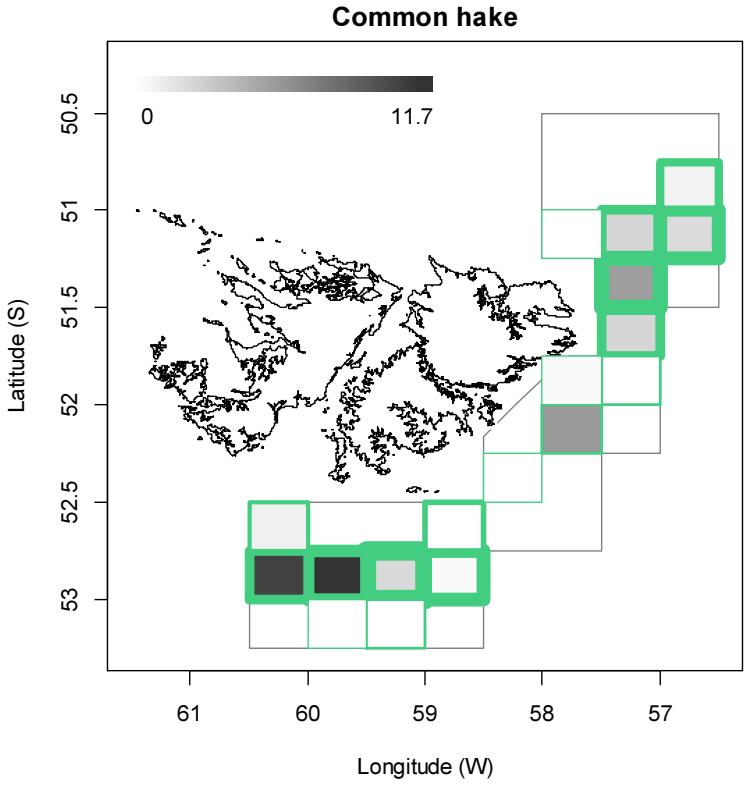

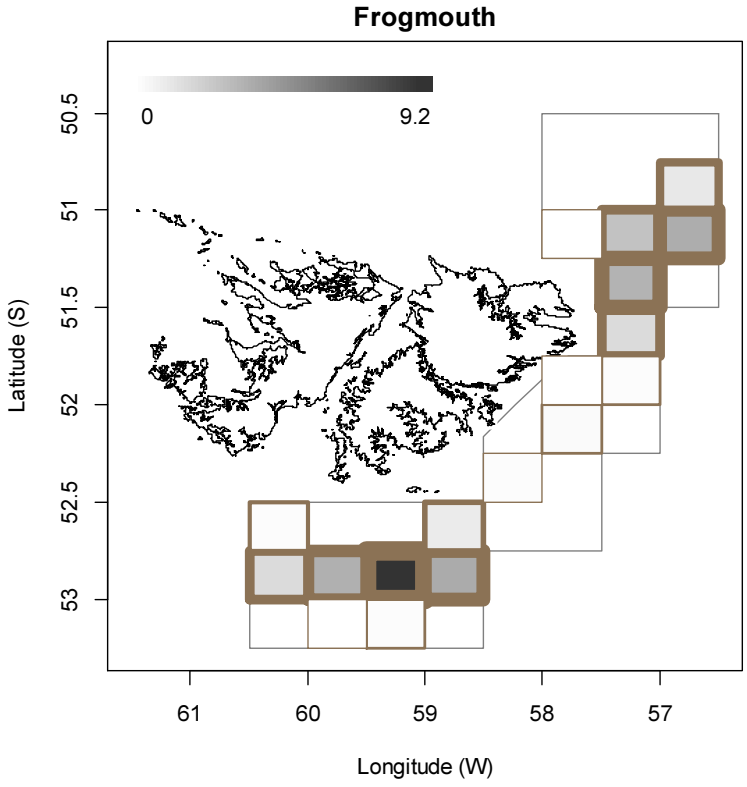

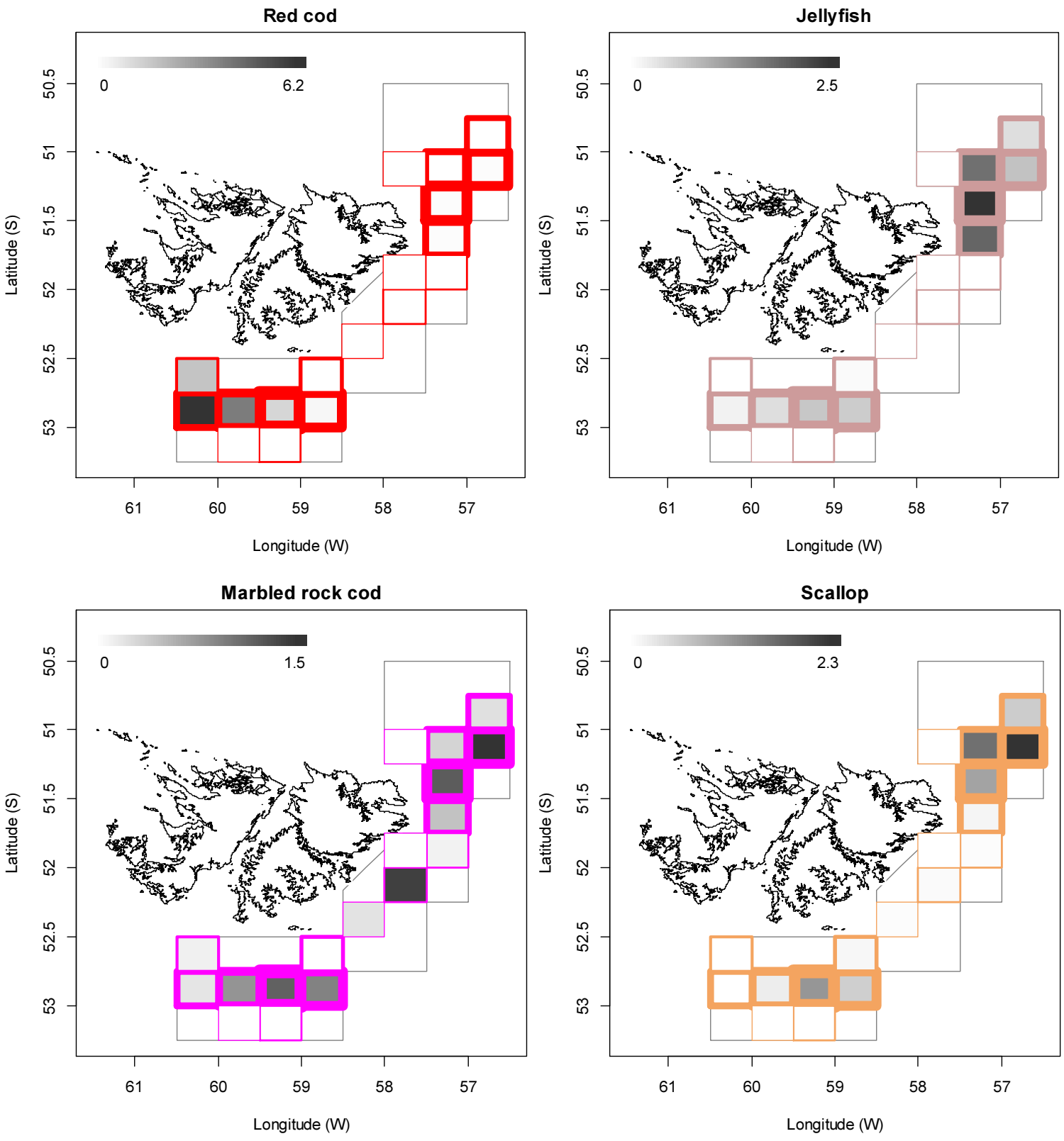

Figure 13. Distributions of the eight principal bycatches during 1st season 2021, by noon position grids. Thickness of grid lines is proportional to the number of vessel-days (1 to 213 per grid; 18 different grids were occupied). Grey-scale is proportional to the bycatch biomass; maximum (tonnes) indicated on each plot.

All of the 891 second season vessel-days (Table 1) reported *D. gahi* squid as their primary catch. The proportion of season total catch represented by *D. gahi* (59587307/60617616 = 0.983; Table A1) is the second-highest for a first season since 2005; after 2019. Highest bycatches in first season 2021 were common rock cod *Patagonotothen ramsayi* with 581 tonnes from 883 vessel-days, shortfin squid *Illex argentinus* (308 t, 617 v-days), common hake *Merluccius hubbsi* (45 t, 374 v-days), frogmouth *Cottoperca gobio* (32 t, 789 v-days), red cod *Salilota australis* (14 t, 210 v-days), jellyfish Medusae (9 t, 93 v-days), marbled rock cod *Patagonotothen tessellata* (9 t, 164 v-days), and scallops probably *Zygochlamys* (8 t, 217 v-days). Relative distributions by grid of these bycatches are shown in Figure 13; the complete list of all catches by species is in Table A1.

Trawl area coverage

The impact of bottom trawling on seafloor habitat has been a matter of concern in commercial fisheries (Kaiser et al. 2002; 2006), whereby the potential severity of impact relates to spatial and temporal extents of trawling (Piet and Hintzen 2012, Gerritsen et al. 2013), as well as the type of trawl gear (Rijnsdorp et al. 2020). For the *D. gahi* fishery, available catch, effort, and positional data are used to summarize the estimated 'ground' area coverage[e] occupied during the season of trawling.

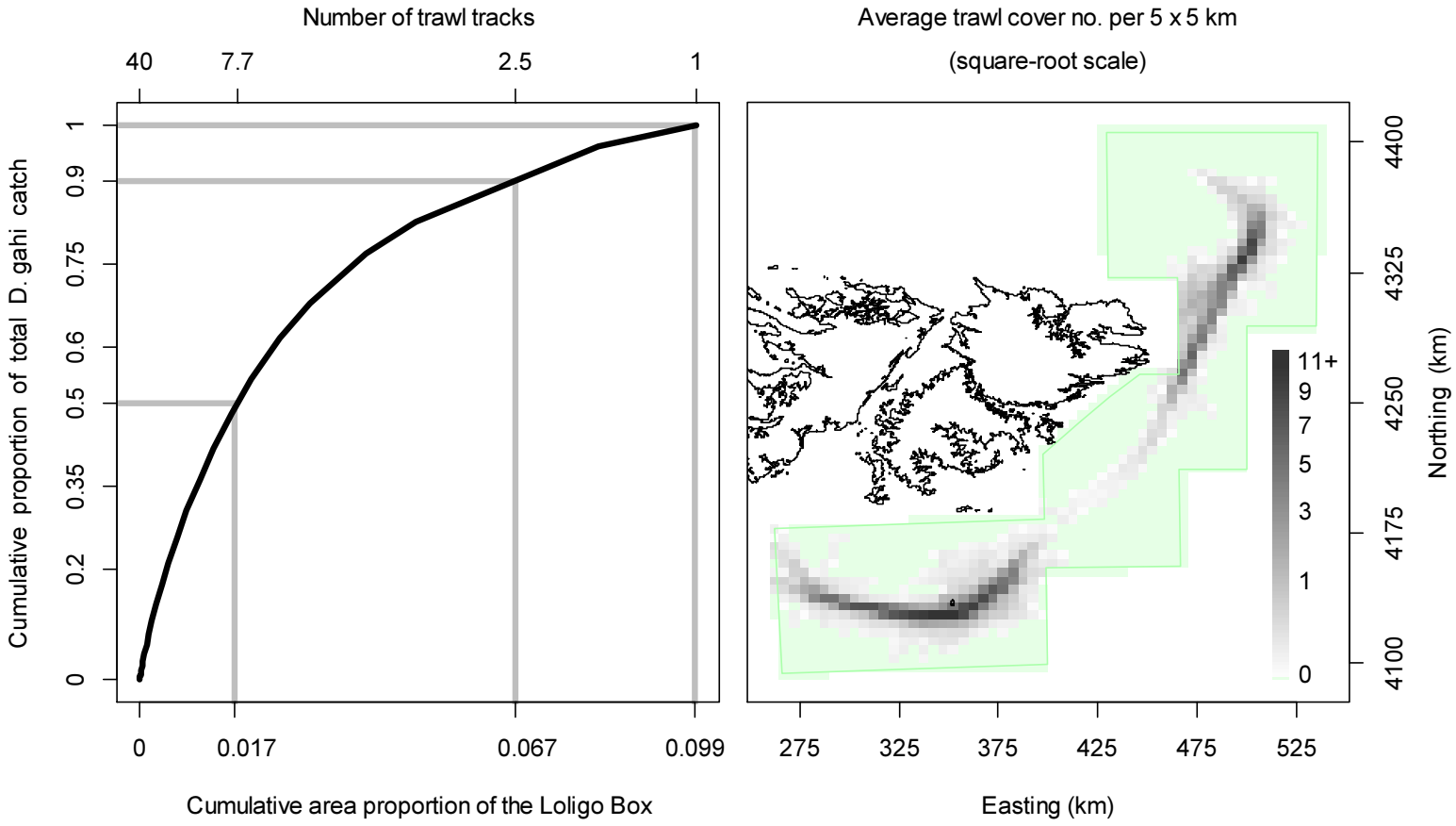

[e] Appropriate spatial scale for calculating area coverage is a matter of some debate (Amoroso et al. 2018, Kroodsma et al. 2018). Given the comparatively small area of the Loligo Box, a high resolution of 5 km × 5 km was used for these calculations.

Figure 14 [previous page]. Left: cumulative *D. gahi* catch of 1st season 2021, vs. cumulative area proportion of the Loligo Box the catch was taken from. The maximum number of times that any single area unit was trawled was 40, and catch cumulation by reverse density corresponded approximately to the trawl multiples shown on the top x-axis. Right: trawl cover averaged by 5 × 5 km grid; green area represents zero trawling.

The procedure for summarizing trawl area coverage is described in the Appendix of the second season 2019 report (Winter 2019b). In first season 2021 50% of total *D. gahi* catch was taken from 1.7% of the total area of the Loligo Box, corresponding approximately[f] to the aggregate of grounds trawled ≥7.7 times. 90% of total *D. gahi* catch was taken from 6.7% of the total area of the Loligo Box, corresponding approximately to the aggregate of grounds trawled ≥2.5 times. 100% of total *D. gahi* catch over the season was taken from 9.9% of the total area of the Loligo Box, obviously corresponding to the aggregate of all grounds trawled at least once (Figure 14 - left). Averaged by 5 × 5 km grid (Figure 14 - right), 5 grids (out of 1383) had coverage of 10 or more (that is to say, every patch of ground within that 5 × 5 km was on average trawled over 10 times or more). Thirty-two grids had coverage of 5 or more, and 80 grids had coverage of 2 or more.

References

Agnew, D.J., Baranowski, R., Beddington, J.R., des Clers, S., Nolan, C.P. 1998. Approaches to assessing stocks of *Loligo gahi* around the Falkland Islands. Fisheries Research 35: 155-169.

Agnew, D. J., Beddington, J. R., and Hill, S. 2002. The potential use of environmental information to manage squid stocks. Canadian Journal of Fisheries and Aquatic Sciences, 59: 1851–1857.

Akaike, H. 1973. Information theory and an extension of the maximum likelihood principle. 2nd International Symposium on Information Theory: 267-281.

Amoroso, R.O., Parma, A.M., Pitcher, C.R., McConnaughey, R.A., Jennings, S. 2018. Comment on "Tracking the global footprint of fisheries". Science 361: eaat6713.

Arkhipkin, A. 1993. Statolith microstructure and maximum age of *Loligo gahi* (Myopsida: Loliginidae) on the Patagonian Shelf. Journal of the Marine Biological Association of the UK 73: 979-982.

Arkhipkin, A.I., Middleton, D.A.J. 2002. Sexual segregation in ontogenetic migrations by the squid *Loligo gahi* around the Falkland Islands. Bulletin of Marine Science 71: 109-127.

Arkhipkin, A.I., Middleton, D.A.J., Barton, J. 2008. Management and conservation of a short-lived fishery resource: *Loligo gahi* around the Falkland Islands. American Fisheries Society Symposium 49: 1243-1252.

Arkhipkin, A.I., Hendrickson, L.C., Payá, I., Pierce, G.J., Roa-Ureta, R.H., Robin, J.-P., Winter, A. 2020. Stock assessment and management of cephalopods: advances and challenges for short-lived fishery resources. ICES Journal of Marine Science, doi:10.1093/icesjms/fsaa038.

[f] However, not exactly. There is an expected strong correlation between the density of *D. gahi* catch taken from area units and how often these area units were trawled, but the correlation is not perfectly monotonic.

Barton, J. 2002. Fisheries and fisheries management in Falkland Islands Conservation Zones. Aquatic Conservation: Marine and Freshwater Ecosystems 12: 127–135.

Brewin, J. 2021. Observer Report 1287. Technical Document, FIG Fisheries Department. 31 p.

Brooks, S.P., Gelman, A. 1998. General methods for monitoring convergence of iterative simulations. Journal of computational and graphical statistics 7:434-455.

Carlson, J.E. 2014. A generalization of Pythagoras's theorem and application to explanations of variance contributions in linear models. Research Report No. RR-14-18, Princeton, NJ: Educational Testing Service. 17 p.

Claes, J. 2021. Observer Report 1289. Technical Document, FIG Fisheries Department. 32 p.

DeLury, D.B. 1947. On the estimation of biological populations. Biometrics 3: 145-167.

Evans, D. 2021. Observer Report 1285. Technical Document, FIG Fisheries Department. 21 p.

FIFD. 2004. Fishery Report, *Loligo gahi*, Second Season 2004. Fishing statistics, biological trends, and stock assessment. Technical Document, Falkland Islands Fisheries Department. 15 p.

Gamerman, D., Lopes, H.F. 2006. Markov Chain Monte Carlo. Stochastic simulation for Bayesian inference. 2nd edition. Chapman & Hall/CRC.

Gerritsen, H.D., Minto, C., Lordan, C. 2013. How much of the seabed is impacted by mobile fishing gear? Absolute estimates from Vessel Monitoring System (VMS) point data. ICES Journal of Marine Science 70: 523-531.

Hoenig, J.M. 1983. Empirical use of longevity data to estimate mortality rates. Fishery Bulletin 82: 898-903

Iriarte, V., Arkhipkin, A., Blake, D. 2020. Implementation of exclusion devices to mitigate seal (*Arctocephalus australis*, *Otaria flavescens*) incidental mortalities during bottom-trawling in the Falkland Islands (Southwest Atlantic). Fisheries Research 227: 105537, 12 p.

Kaiser, M.J., Collie, J.S., Hall, S.J., Jennings, S., Poiner, I.R. 2002. Modification of marine habitats by trawling activities: prognosis and solutions. Fish and Fisheries 3: 114-136.

Kaiser, M.J., Clarke, K.R., Hinz, H., Austen, M.C.V., Somerfield, P.J., Karakassis, I. 2006. Global analysis of response and recovery of benthic biota to fishing. Marine Ecology Progress Series 311: 1-14.

Kroodsma, D.A., Mayorga, J., Hochberg, T., Miller, N.A., Boerder, K., Ferretti, F., Wilson, A., Bergman, B., White, T.D., Block, B.A., Woods, P., Sullivan, B., Costello, C., Worm, B. 2018. Response to Comment on "Tracking the global footprint of fisheries". Science 361: eaat7789.

Lipiński, M. R. 1979. Universal maturity scale for the commercially important squids (Cephalopoda: Teuthoidea). The results of maturity classification of *Illex illecebrosus* (Le Sueur 1821) population for years 1973–1977. ICNAF Research Document 79/11/38, 40 p.

Magnusson, A., Punt, A., Hilborn, R. 2013. Measuring uncertainty in fisheries stock assessment: the delta method, bootstrap, and MCMC. Fish and Fisheries 14: 325-342.

Nash, J.C., Varadhan, R. 2011. optimx: A replacement and extension of the optim() function. R package version 2011-2.27. http://CRAN.R-project.org/package=optimx

Patterson, K.R. 1988. Life history of Patagonian squid *Loligo gahi* and growth parameter estimates using least-squares fits to linear and von Bertalanffy models. Marine Ecology Progress Series 47: 65-74.

Payá, I. 2006. Fishery Report. *Loligo gahi*, Second Season 2006. Fishery statistics, biological trends, stock assessment and risk analysis. Technical Document, Falkland Islands Fisheries Dept. 40 p.

Payá, I. 2010. Fishery Report. *Loligo gahi*, Second Season 2009. Fishery statistics, biological trends, stock assessment and risk analysis. Technical Document, Falkland Islands Fisheries Dept. 54 p.

Pierce, G.J., Guerra, A. 1994. Stock assessment methods used for cephalopod fisheries. Fisheries Research 21: 255–285.

Piet, G.J., Hintzen, N.T. 2012. Indicators of fishing pressure and seafloor integrity. ICES Journal of Marine Science 69: 1850-1858.

Plet-Hansen, K.S., Larsen, E., Mortensen, L.O., Nielsen, J.R., Ulrich, C. 2018. Unravelling the scientific potential of high resolution fishery data. Aquatic Living Resources 31:24.

Punt, A.E., Hilborn, R. 1997. Fisheries stock assessment and decision analysis: the Bayesian approach. Reviews in Fish Biology and Fisheries 7:35-63.

Rijnsdorp, A.D., Hiddink, J.G., van Denderen, P.D., Hintzen, N.T., Eigaard, O.R., Valanko, S., Bastardie, F., Bolam, S.G., Boulcott, P., Egekvist, J., Garcia, C., van Hoey, G., Jonsson, P., Laffargue, P., Nielsen, J.R., Piet, G.J., Sköld, M., van Kooten, T. 2020. Different bottom trawl fisheries have a differential impact on the status of the North Sea seafloor habitats. ICES Journal of Marine Science 77: 1772–1786.

Roa-Ureta, R. 2012. Modelling in-season pulses of recruitment and hyperstability-hyperdepletion in the *Loligo gahi* fishery around the Falkland Islands with generalized depletion models. ICES Journal of Marine Science 69: 1403–1415.

Roa-Ureta, R., Arkhipkin, A.I. 2007. Short-term stock assessment of *Loligo gahi* at the Falkland Islands: sequential use of stochastic biomass projection and stock depletion models. ICES Journal of Marine Science 64: 3-17.

Rohlf, F.J., Sokal, R.R. 1981. Statistical Tables, Second Edition. W.H. Freeman and Co., NY, 219 p.

Rosenberg, A.A., Kirkwood, G.P., Crombie, J.A., Beddington, J.R. 1990. The assessment of stocks of annual squid species. Fisheries Research 8: 335-350.

Shaw, P.W., Arkhipkin, A.I., Adcock, G.J., Burnett, W.J., Carvalho, G.R., Scherbich, J.N., Villegas, P.A. 2004. DNA markers indicate that distinct spawning cohorts and aggregations of Patagonian squid, *Loligo gahi*, do not represent genetically discrete subpopulations. Marine Biology, 144: 961-970.

Swartzman, G., Huang, C., Kaluzny, S. 1992. Spatial analysis of Bering Sea groundfish survey data using generalized additive models. Canadian Journal of Fisheries and Aquatic Sciences 49: 1366-1378.

Tutjavi, V. 2021. Observer Report 1292. Technical Document, FIG Fisheries Department. 27 p.

Winter, A. 2011. *Loligo gahi* stock assessment, First season 2011. Technical Document, Falkland Islands Fisheries Department. 23 p.

Winter, A. 2014. *Loligo* stock assessment, second season 2014. Technical Document, Falkland Islands Fisheries Department. 30 p.

Winter, A. 2015. *Loligo* stock assessment, first season 2015. Technical Document, Falkland Islands Fisheries Department. 28 p.

Winter, A. 2019a. Stock assessment –Falkland calamari *Doryteuthis gahi* 1st season 2019. Technical Document, Falkland Islands Fisheries Department. 37 p.

Winter, A. 2019b. Stock assessment –Falkland calamari *Doryteuthis gahi* 2nd season 2019. Technical Document, Falkland Islands Fisheries Department. 36 p.

Winter, A. 2020. Stock assessment –Falkland calamari *Doryteuthis gahi* 1st season 2020. Technical Document, Falkland Islands Fisheries Department. 34 p.

Winter, A., Arkhipkin, A. 2015. Environmental impacts on recruitment migrations of Patagonian longfin squid (*Doryteuthis gahi*) in the Falkland Islands with reference to stock assessment. Fisheries Research 172: 85-95.

Winter, A., Shcherbich, Z., Matošević, N. 2021. Falkland calamari (*Doryteuthis gahi*) stock assessment survey, 1st season 2021. Technical Document, Falkland Islands Fisheries Department. 18 p.

Appendix
***Doryteuthis gahi* individual weights**

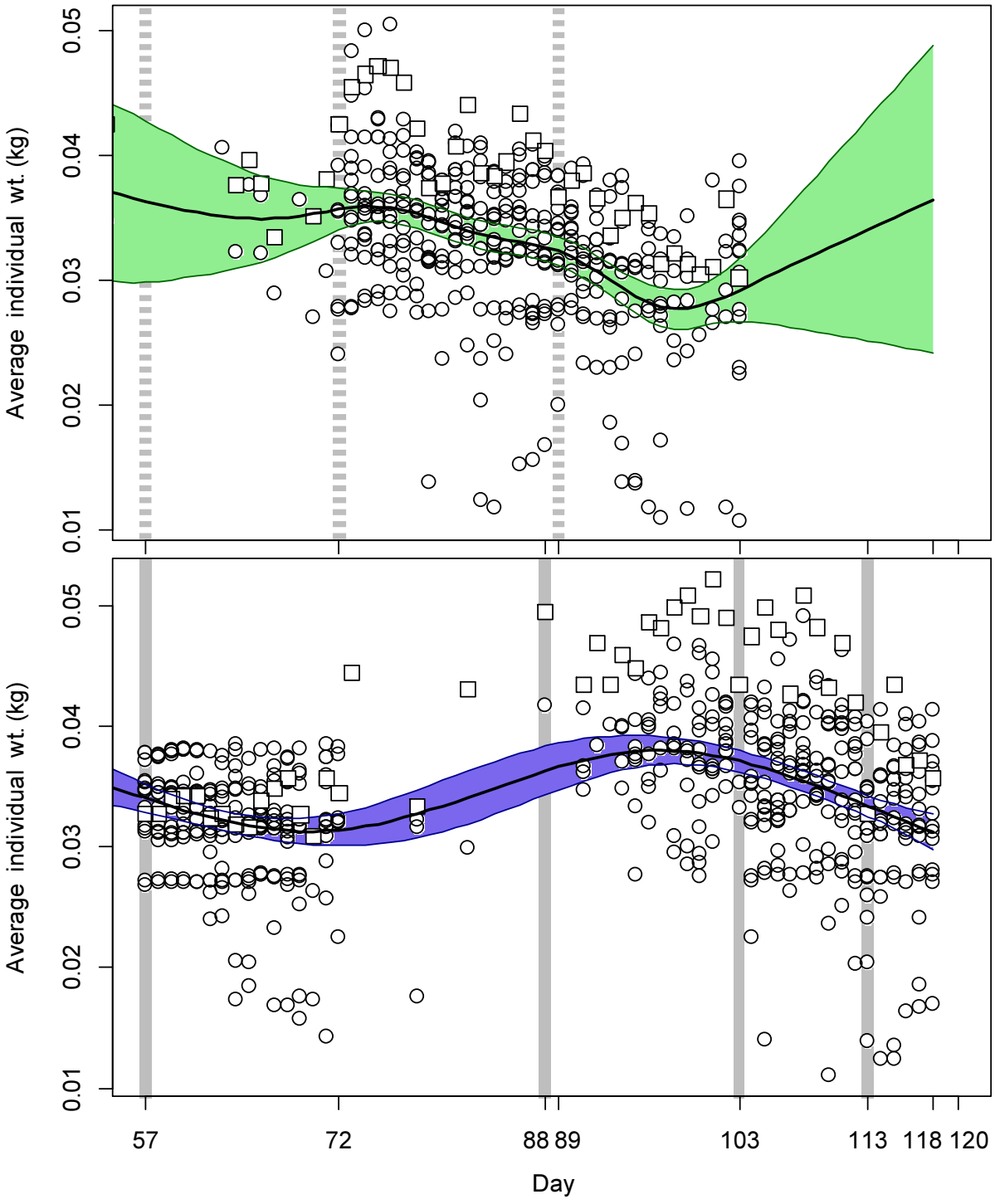

Figure A1. North (top) and south (bottom) sub-area daily average individual *D. gahi* weights from commercial size categories per vessel (circles) and observer measurements (squares). GAMs of the daily trends ± 95% confidence interval (centre lines and colour under-shading).

To smooth fluctuations, GAM trends were calculated of daily average individual weights. North and south sub-areas were calculated separately. For continuity, GAMs were calculated

using all pre-season survey and in-season data contiguously. North and south GAMs were first calculated separately on the commercial and observer data. Commercial data GAMs were taken as the baseline trends, and calibrated to observer data GAMs in proportion to the correlation between commercial data and observer data GAMs. For example, if the season average individual weight estimate from commercial data was 0.052 kg, the season average individual weight estimate from observer data was 0.060 kg, and the coefficient of determination (R^2) between commercial and observer GAM trends was 86%, then the resulting trend of daily average individual weights was calculated as the commercial data GAM values + (0.060 – 0.052) × 0.86. This way, both the greater day-to-day consistency of the commercial data trends, and the greater point value accuracy of the observer data are represented in the calculations. GAM plots of the north and south sub-areas are in Figure A1.

Prior estimates and CV

The pre-season survey had estimated *D. gahi* biomass of 31,770 tonnes (Winter et al. 2021). Hierarchical bootstrapping of the inverse distance weighting algorithm obtained a coefficient of variation (CV) equal to 15.6% of the survey biomass distribution. From modelled survey catchability, Payá (2010) had estimated average net escapement of up to 22%, which was added to the CV:

$$31{,}770 \pm (.156 + .22) = 31{,}770 \pm 37.6\% = 31{,}770 \pm 11{,}934 \text{ t} \quad \textbf{(A1)}$$

The 22% escapement was added as a linear increase in the variability, but was not used to reduce the total estimate, because squid that escape one trawl are likely to be part of the biomass concentration that is available to the next trawl.

D. gahi numbers from the survey were estimated as the survey biomasses divided by the GAM-predicted individual weight average for the survey: 0.0375 kg. The average coefficient of variation (CV) of the GAM over the duration of the pre-season survey was 3.6%, and CV of the length-weight conversion relationship (Equation **7**) was 8.7%. Joining these sources of variation with the pre-season survey biomass estimates and individual weight averages (above) gave estimated *D. gahi* numbers at survey end (day 54) of:

$$\begin{aligned} {}_{\text{prior}}\text{N}_{\text{day 54}} &= \frac{31{,}770 \times 1000}{0.0375} \pm \sqrt{37.6\%^2 + 3.6\%^2 + 8.7\%^2} \\ &= 0.847 \times 10^9 \pm 38.7\% \end{aligned} \quad \textbf{(A2)}$$

The combined catchability coefficient (q) prior was taken on day 57, the first day of the season, when 14 vessels fished in the south sub-area (Figure 5). Abundance on day 57 was discounted for natural mortality over the 3 days since the end of the survey:

$${}_{\text{prior}}\text{N}_{\text{day 57}} = {}_{\text{prior}}\text{N}_{\text{S day 54}} \times e^{-M\cdot(57-54)} - \text{CNMD}_{\text{day 57}} = 0.814 \times 10^9 \quad \textbf{(A3)}$$

where $\text{CNMD}_{\text{day 57}} = 0$ as no catches intervened between the end of the survey and the start of commercial season. Thus:

$$\begin{aligned} {}_{\text{prior}}\text{q} &= \text{C(N)}_{\text{day 57}} / ({}_{\text{prior}}\text{N}_{\text{day 57}} \times \text{E}_{\text{day 57}}) \\ &= (\text{C(B)}_{\text{day 57}} / \text{Wt}_{\text{day 57}}) / ({}_{\text{prior}}\text{N}_{\text{day 57}} \times \text{E}_{\text{S day 57}}) \end{aligned}$$

$$= (1005.3 \text{ t} / 0.03404 \text{ kg}) / (0.814 \times 10^9 \times 14 \text{ vessel-days})$$

$$= 2.591 \times 10^{-3} \text{ vessels}^{-1}\ ^{g} \quad \textbf{(A4)}$$

$SD_{\text{prior q}}$ (Equation **4**) was calculated as $_{\text{prior}}q$ multiplied by its CV. $CV_{\text{prior q}}$ was calculated as the sum of variability in $_{\text{prior}}N_{\text{day 57}}$ (Equation **A2**) plus variability in the catches of vessels on start day 57, plus variability of the natural mortality (see Appendix section Natural mortality).

$$CV_{\text{prior q}} = \sqrt{38.7\%^2 + \left(\frac{SD\left(C(B)_{\text{vessels day 57}}\right)}{\text{mean}\left(C(B)_{\text{vessels day 57}}\right)}\right)^2 + \left(1 - (1 - CV_M)^{(57 - \text{mid\_survey})}\right)^2}$$

$$= \sqrt{38.7\%^2 + 17.7\%^2 + 80.1\%^2} = 90.7\%$$

$$SD_{\text{prior q}} = {}_{\text{prior}}q \times CV_{\text{prior q}} = 2.351 \times 10^{-3} \text{ vessels}^{-1} \quad \textbf{(A5)}$$

Depletion model estimates and CV

For the south sub-area, the equivalent of Equation **2** with four N_{day} was optimized on the difference between predicted and actual catches (Equation **3**), resulting in parameters values:

$_{\text{depletion}}N1_{\text{S day 57}} = 1.439 \times 10^9$; $_{\text{depletion}}N2_{\text{S day 88}} = 0.709 \times 10^6$

$_{\text{depletion}}N3_{\text{S day 103}} = 0.484 \times 10^9$; $_{\text{depletion}}N4_{\text{S day 113}} = 0.707 \times 10^6$

$_{\text{depletion}}q_{\text{S}} = 1.556 \times 10^{-3}$ [h] **(A6-S)**

For the north sub-area, the Equation **2** equivalent with three N_{day} was optimized on the difference between predicted and actual catches (Equation **3**), resulting in parameter values:

$_{\text{depletion}}N1_{\text{N day 57}} = 1.021 \times 10^9$; $_{\text{depletion}}N2_{\text{N day 72}} = 2.518 \times 10^9$

$_{\text{depletion}}N3_{\text{N day 89}} = 1.449 \times 10^9$

$_{\text{depletion}}q_{\text{N}} = 0.661 \times 10^{-3}$ [i] **(A6-N)**

Combined Bayesian models

For the south sub-area, joint optimization of Equations **3** and **4** resulted in parameters values:

$_{\text{Bayesian}}N1_{\text{S day 57}} = 1.155 \times 10^9$; $_{\text{Bayesian}}N2_{\text{S day 88}} = 0.572 \times 10^9$

$_{\text{Bayesian}}N3_{\text{S day 103}} = 0.416 \times 10^9$; $_{\text{Bayesian}}N4_{\text{S day 113}} = 0.593 \times 10^9$

$_{\text{Bayesian}}q_{\text{S}} = 2.063 \times 10^{-3}$ [j] **(A7-S)**

[g] On Figure 8-left and Figure 10-left.
[h] On Figure 8-left.
[i] On Figure 10-left.
[j] On Figure 8-left.

These parameters produced the fit between predicted catches and actual catches shown in Figure A2-S.

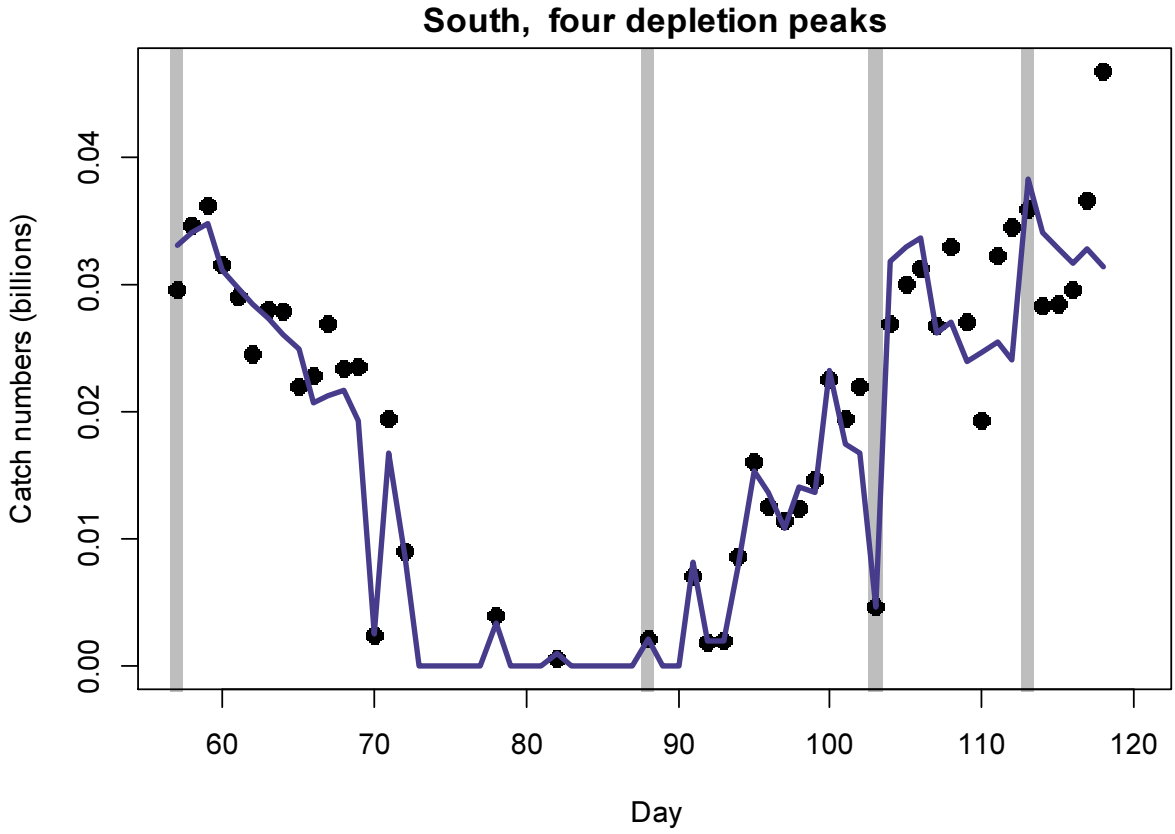

Figure A2-S. Daily catch numbers estimated from actual catch (black points) and predicted from the depletion model (purple line) in the south sub-area.

For the north sub-area, joint optimization of Equations **3** and **4** resulted in parameters values:

$_{\text{Bayesian}}N1_{\text{N day 57}} = 0.334 \times 10^{9}$; $_{\text{Bayesian}}N2_{\text{N day 72}} = 0.993 \times 10^{9}$

$_{\text{Bayesian}}N3_{\text{N day 89}} = 0.737 \times 10^{9}$

$_{\text{Bayesian}}q_{\text{N}} = 2.030 \times 10^{-3}$ [k] **(A7-N)**

These parameters produced the fit between predicted catches and actual catches shown in Figure A2-N.

Figure A2-N [next page]. Daily catch numbers estimated from actual catch (black points) and predicted from the depletion model (green line) in the north sub-area.

[k] On Figure 10-left.

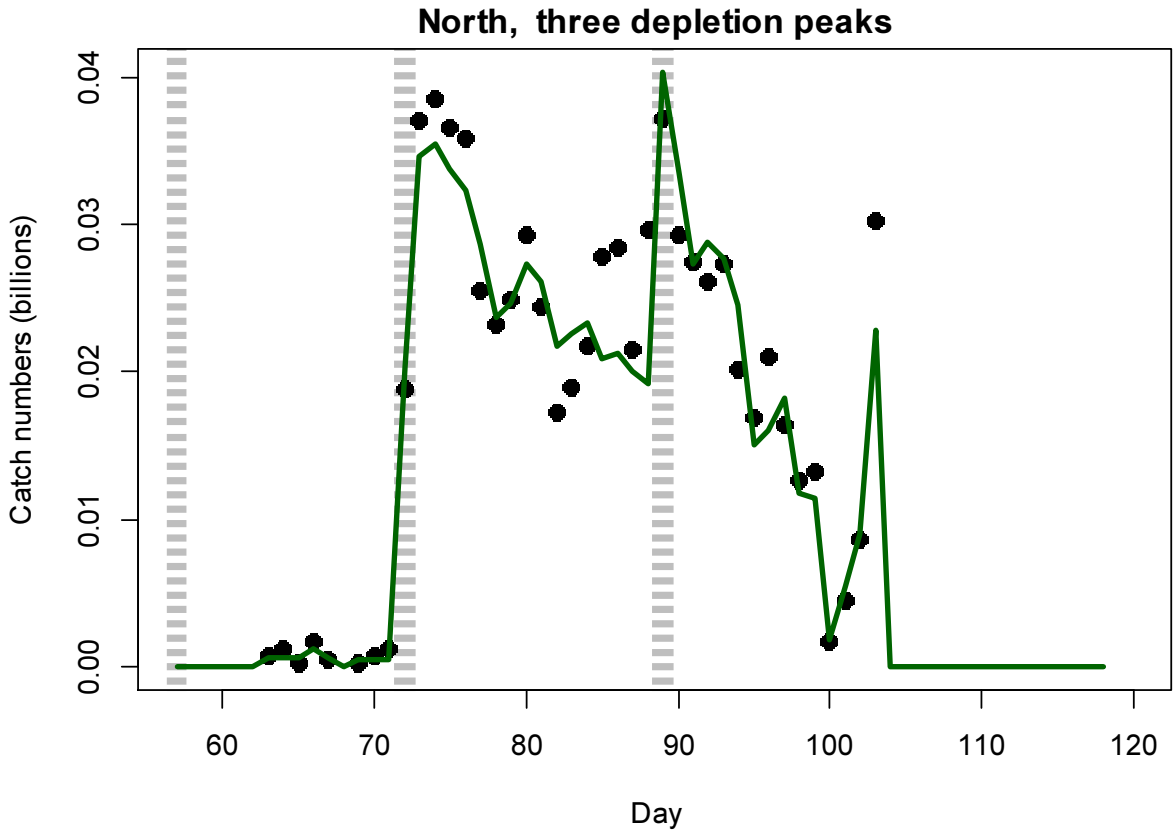

Natural mortality

Natural mortality is parameterized as a constant instantaneous rate M = 0.0133 day^{-1} (Roa-Ureta and Arkhipkin 2007), based on Hoenig's (1983) log mortality vs. log maximum age regression, applied to an estimated maximum age of 352 days for *D. gahi*:

$$\log(M) = 1.44 - 0.982 \times \log(age_{max})$$

$$M = \exp(1.44 - 0.982 \times \log(352))$$

$$= 0.0133 \quad \textbf{(A8)}$$

Hoenig (1983) derived Equation **A8** from the regression of 134 stocks among 79 species of fish, molluscs, and cetaceans. Hoenig's regression obtained $R^2 = 0.82$, but a corresponding coefficient of variation (CV) was not published. An approximate CV of M was estimated by measuring the coordinates off a print of Figure 1 in Hoenig (1983) and repeating the regression. Variability of M was calculated by randomly re-sampling, with replacement, the regression coordinates 10000× and re-computing Equation **A8** for each iteration of the resample. The CV of M from the 10000 random resamples was:

$$CV_M = SD_M / Mean_M$$

$$CV_M = 0.0021 / 0.0134 = 15.46\% \quad \textbf{(A9)}$$

The algorithm was modified this season by aggregating CV_M over the number of days between the midpoint of the survey and the commercial season start, rather than between the end of the survey and commercial season start, as the midpoint more accurately reflects how much time has elapsed since the fishing area on average was surveyed. The midpoint of the survey was calculated as the mean day weighted by the number of survey trawls taken per day:

$$\text{mid\_survey} = \frac{\Sigma\left(\text{day} \times N_{\text{survey trawls}}|_{\text{day}}\right)}{\Sigma\left(N_{\text{survey trawls}}|_{\text{day}}\right)} = 47.4^{[l]} \quad \textbf{(A10)}$$

CV_M was thus further indexed by $1 - (1 - CV_M)$ to ensure that the value could not decrease if CV_M was hypothetically > 100%:

$$1 - (1 - CV_M)^{(\text{commercial season start} - \text{mid\_survey})} \quad \textbf{(A11)}$$

Equation **A11** is included in Equation **A5**.

Individual weight uncertainty

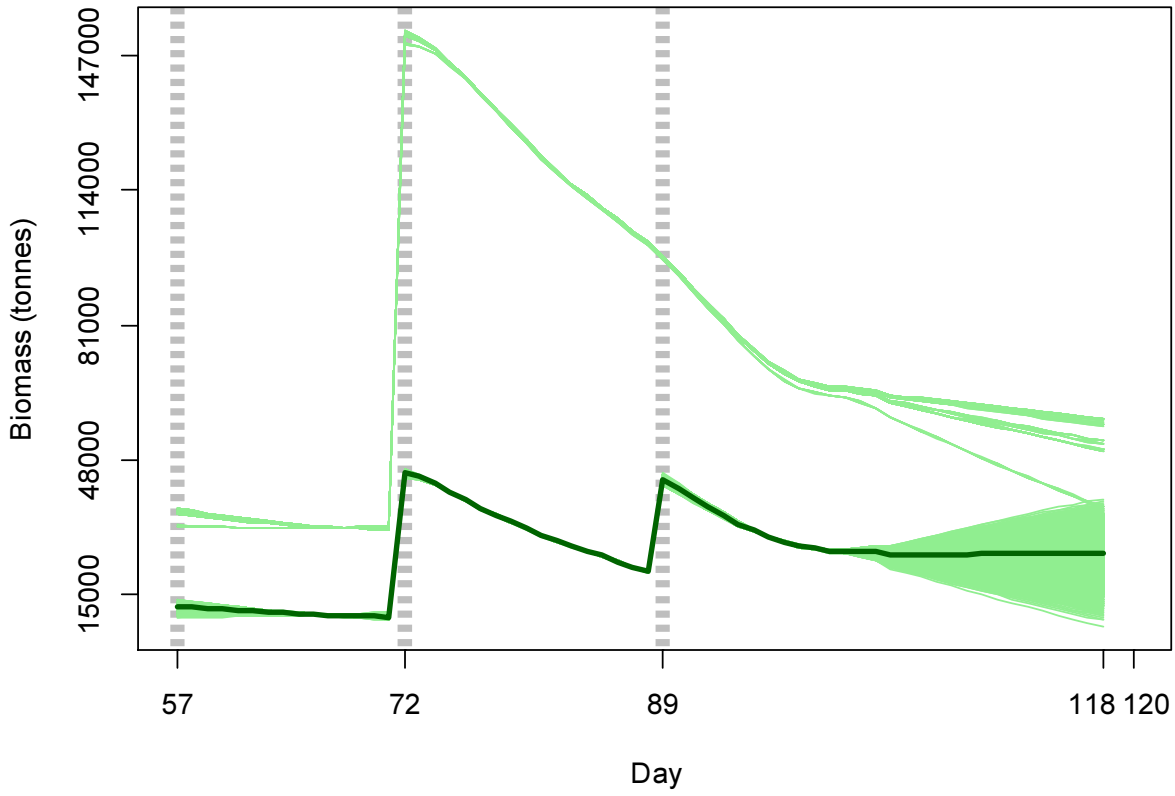

Figure A3-N. Iterations of the north sub-area biomass time series with randomly resampled average individual weights. Dark green line: empirical maximum likelihood biomass estimate, equivalent to the dark green line in Figure 11.

[l] In common nomenclature day 47 and day 48 are February 16th and February 17th.

To account for the wide uncertainty of average individual weight in the north sub-area, especially at the start and end of the season (Figure A1), average individual weights were randomly resampled on the normal distribution and biomasses recalculated. North sub-area biomass time series with randomized resampled average weights are shown in Figure A3-N. Of 30,000 iterations, one iteration failed to converge. 109 iterations converged on much higher average biomasses, and were not included in the added variance estimation. The added variance produced by the remaining 29,890 iterations increased the width of the 95% confidence interval of the biomass time series between <0.01% and 9.6%. The increased 95% confidence interval is included in Figures 10-right, 11 and 12.

Total catch by species

Table A1: Total reported catches and discard by taxon during 1st season 2021 C-license fishing, and number of catch reports in which each taxon occurred. Does not include incidental catches of pinnipeds or seabirds.

Species Code	Species / Taxon	Catch Wt. (KG)	Discard Wt. (KG)	N Reports
LOL	*Doryteuthis gahi*	59587307	55456	891
PAR	*Patagonotothen ramsayi*	581262	580153	883
ILL	*Illex argentinus*	307669	36908	617
HAK	*Merluccius hubbsi*	45068	7258	374
CGO	*Cottoperca gobio*	32232	32217	789
BAC	*Salilota australis*	13703	2157	210
MED	Medusae sp.	9316	11626	93
PTE	*Patagonotothen tessellata*	8600	8600	164
SCA	Scallop	7756	7756	217
RAY	Rajiformes	7546	7328	554
KIN	*Genypterus blacodes*	4569	2103	188
TOO	*Dissostichus eleginoides*	3776	3070	263
DGH	*Schroederichthys bivius*	2323	2323	226
ING	*Moroteuthis ingens*	1431	1427	180
CHE	*Champsocephalus esox*	1236	1236	134
UCH	Sea urchin	844	844	35
OCT	*Octopus* spp.	648	646	136
ALF	*Allothunnus fallai*	478	478	50
POR	*Lamna nasus*	461	461	8
WHI	*Macruronus magellanicus*	444	444	71
GRF	*Coelorhynchus fasciatus*	356	356	20
GRV	*Macrourus* spp.	182	182	35
SPN	Porifera	173	173	17
MYX	*Myxine* spp.	105	105	19
NEM	*Neophyrnichthys marmoratus*	25	25	10
BLU	*Micromesistius australis*	18	18	6
MAR	*Martialia hyadesi*	15	15	1
DGX	Dogfish / Catshark	12	12	1
MUL	*Eleginops maclovinus*	11	11	5
EEL	*Iluocoetes fimbriatus*	9	9	7
SAR	*Sprattus fuegensis*	8	8	1
LIM	*Lithodes murrayi*	8	8	2
DGS	*Squalus acanthias*	6	6	2
PAT	*Merluccius australis*	5	5	3

PRO	*Procellaria aequinoctialis*	4	3	4
BDU	*Brama dussumieri*	3	3	1
RED	*Sebastes oculatus*	2	2	1
SEP	*Seriolella porosa*	2	2	1
BUT	*Stromateus brasiliensis*	1	1	1
COP	*Congiopodus peruvianus*	1	1	1
COT	*Cottunculus granulosus*	1	1	1
Total		60617616	763437	891